②

AFOSR-TR. 90-0085

AD-A218 068

AIR FORCE OFFICE OF SCIENTIFIC RESEARCH (AFSC)
NOTICE OF TRANSMITTAL TO DTIC
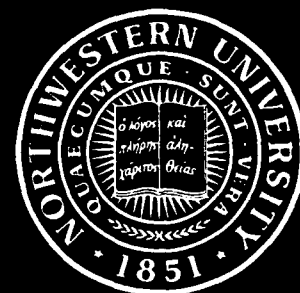This technical report has been reviewed and is
approved for public release IAW AFR 190-12.
Distribution is unlimited.
MATTHEW J. KERPER
Chief, Technical Information Division

Technological Institute
NORTHWESTERN UNIVERSITY
EVANSTON, ILLINOIS

FINAL REPORT

A STUDY OF FRACTURE PROCESSES IN CONCRETE
USING LASER HOLOGRAPHY

AFOSR - F49620-88-C-0118

PRINCIPAL INVESTIGATOR: S. P. SHAH

DTIC
ELECTE
FEB07 1990
S B D

90 0: 06 151

REPORT DOCUMENTATION PAGE

1a. REPORT SECURITY CLASSIFICATION	1b. RESTRICTIVE MARKINGS
- Unclassified	

2a. SECURITY CLASSIFICATION AUTHORITY	3. DISTRIBUTION/AVAILABILITY OF REPORT
	Approved for Public Release
2b. DECLASSIFICATION/DOWNGRADING SCHEDULE	Distribution Unlimited

4. PERFORMING ORGANIZATION REPORT NUMBER(S)	5. MONITORING ORGANIZATION REPORT NUMBER(S)

6a. NAME OF PERFORMING ORGANIZATION	6b. OFFICE SYMBOL (If applicable)	7a. NAME OF MONITORING ORGANIZATION
Northwestern University Department of Civil Engineering		AFOSR/NA

6c. ADDRESS (City, State and ZIP Code)	7b. ADDRESS (City, State and ZIP Code)
Evanston, Illinois 60201	Bolling AFB Washington DC 20332-6448

8a. NAME OF FUNDING/SPONSORING ORGANIZATION AIR FORCE Office of Scientific Research	8b. OFFICE SYMBOL (If applicable) AFOSR/NA	9. PROCUREMENT INSTRUMENT IDENTIFICATION NUMBER F49620-88-C-0118

8c. ADDRESS (City, State and ZIP Code)	10. SOURCE OF FUNDING NOS			
Bolling Air Force Base Washington, D. C. 20332	PROGRAM ELEMENT NO	PROJECT NO	TASK NO	WORK UNIT NO
	61102F	2302	C2	

11. TITLE (Include Security Classification) (U) A STUDY OF FRACTURE PROCESS IN CONCRETE USING LASER HOLOGRAPHY

12. PERSONAL AUTHOR(S)
- Surendra P. Shah

13a. TYPE OF REPORT	13b. TIME COVERED	14. DATE OF REPORT (Yr., Mo., Day)	15. PAGE COUNT
Final	FROM 8/88 TO 9/89	December 27, 1989	62

16. SUPPLEMENTARY NOTATION

17.	COSATI CODES		18. SUBJECT TERMS (Continue on reverse if necessary and identify by block number)
FIELD	GROUP	SUB GR	Concrete cracks, Fracture process zone, Laser Holographic Measurements, Mixed Mode cracks.

19. ABSTRACT (Continue on reverse if necessary and identify by block number)

See Executive Summary.

20. DISTRIBUTION/AVAILABILITY OF ABSTRACT	21. ABSTRACT SECURITY CLASSIFICATION
UNCLASSIFIED/UNLIMITED ☒ SAME AS RPT ☐ DTIC USERS ☐	UNCLASSIFIED

22a. NAME OF RESPONSIBLE INDIVIDUAL	22b. TELEPHONE NUMBER (Include Area Code)	22c. OFFICE SYMBOL
Dr. Spencer Wu	(202)767-6962	AFOSR/NA

DD FORM 1473, 83 APR   EDITION OF 1 JAN 73 IS OBSOLETE

TABLE OF CONTENTS

Distribution/
Availability Codes

Dist	Avail and/or Special
A-1	

EXECUTIVE SUMMARY

Conventional linear elastic fracture mechanics cannot explain fracture in concrete and mortar. Unlike traditional LEFM materials which show a constant fracture toughness, concrete and mortar toughen (show more resistance to fracture) as cracks propagate until an instability results and the structure fails. This increase in toughness is thought to occur because of many possible complex mechanisms which take place during fracture in concrete and mortar. These mechanisms include: formation of a zone of microcracking around the crack tip; crack bridging, where aggregate particles span the crack and act as ligaments to hold the crack together; and crack deflection, where the crack changes direction. All of these mechanisms require additional energy input into the system and may explain the apparent toughening of the material.

Cohesive zone models based on the Dugdale-Barrenblatt approach of placing a closing pressure on the faces of a discrete crack could be used to account for the nonlinear effects of the fracture process zone (FPZ). Computer codes based on such concept have been developed. It is generally assumed that the closing pressure is a function of the crack opening displacement (w). Since the results of finite element computations are quite sensitive to the shape of the assumed closing pressure vs. w relationship it is essential to determine such relationship as accurately as possible.

Normally closing pressure vs. w relationships are calibrated by comparing experimentally measured macroscopic displacements (such as load-joint deflection in beam test) with those calculated numerically. Such a procedure does not give a precise or an unique relationship between closing pressure vs. crack opening displacement.

In this study, crack profiles as well as the full field microscopic displacements on the fracture process zone were accurately measured by laser holographic interferometry. With this technique it was possible to measure the two-dimensional displacement field around a crack tip with an accuracy of a quarter of a micron. Such accurate measurement of strain field in FPZ provided a better understanding of the fracture process in concrete.

The first two parts of this report discuss mode I fracture of concrete which was studied using center notched plate specimens. Initially, crack profiles were measured by illuminating the specimens only from a single direction. This was sufficient to obtain crack opening displacements. To obtain 2-D strain field three simultaneous holograms were made by illuminating the specimens from 3 different directions. To analyze three different simultaneous holographic patterns, a digital image analysis technique was developed. The results from holographic study were compared with finite element analysis based on linear elastic fracture mechanics. This comparison permitted a new definition of FPZ as well as more accurate relationship between closing pressure and crack opening displacement.

In the last part of this report, a study of mixed mode crack propagation under compression is described. Mortar plates were subjected to uniaxial compression. These specimens had notched which were inclined from the direction of compression. The crack trajectory and crack opening and sliding displacement were measured with laser holographic interferometry. The results were compared with LEFM solutions obtained using finite element analysis. A cohesive crack model which includes both normal and shear traction was developed for the case of mixed mode crack propagation.

. (R.H)

iii

LIST OF PUBLICATIONS

1. Maji, A.K. and Shah, S.P. "Measurement of Mixed-Mode Crack Profiles by Holographic Interferometry," accepted for publication in <u>Experimental Mechanics, 1990</u>

2. Maji, A.K., Tasdemir, M. and Shah, S.P. "Crack Propagation in Concrete Under Compression," accepted for publication in ASCE Engg. Mechanics Division, 1990

3. Maji, A.K., Tasdemir, M. and Shah, S.P. "Mixed Mode Crack Propagation in Quasi-Brittle Materials," Submited for publication in Engg. Fracutre Mechanics

4. Miler, R.A., Castro-Montero, A. and Shah, S.P. "Cohesive Crack Models Examined with Laser Holographic Interferometry," Submited for publication in The Journal of the American Ceramic Society.

5. Castro-Montero, A., Shah, S.P. and Miller, R.A. "Measurement of Strain Fields in Fracture Process Zone of Mortar," Submited for publication in ASCE- Engg. Mechanics Division

6. John, R. and Shah, S.P. "Fracture Mechanics Analysis of High Strength Concrete," ASCE-Mat. Engg. Division, Vol. 1, No. 4, Nov. 1989

7. John, R. and Shah, S.P. "Mixed Mode Fracture of Concrete Subjected to Impact Loading," accepted for publication in ASCE-Structural Division

8. Labuz, J.F., Shah, S.P. and Dowding, C.H. "Measurement and Description of Tensile Fracture in Granite," ASCE-Engg. Mechanics Division, Vol. 115, No. 9, Sept. 1989

Proceedings

9. Miller, R.A., Castro-Montero, A. and Shah, S.P. "Fracture Process in Concrete Studied by Laser Holography," 1989 SEM Spring Conference on Experimental Mechanics, Cambridge, MA.

10. Maji, A.K., Shah, S.P. and Tasdemir, M.A., "A Study of Mixed mOde Crack Propagation in Mortar Using Holographic Interferometry," 1989 SEM Spring Conference on Experimental Mechanics, Cambridge, MA.

11. Jenq, Y-S and Shah, S.P. "On the Fundamental Issues of Mixed Mode Crack Propagation in Concrete," <u>Fracture of Concrete and Rock</u>, Ed. S.P. Shah, S.E. Swarts and B. Barr, Elsevieer Applied Science.

12. Tasdemir, M.A., Maji, A.K ans Shah, S.P. "Mixed Mode Crack Propagation in Concrete Under Uniaxial Compressive Loading," <u>Fracture of Concrete and Rock</u>, Ed. S.P. Shah, S.E. Swarts and B. Barr, Elsevieer Applied Science.

13. Maji, A.K. and Shah, S.P. "Mixed Mode Fracture in Compression," RILEM workshop dedecated to Prof. Arne Hillerborg, Abisko, Sweden, June 1989

Part I.   COHESIVE CRACK MODELS EXAMINED WITH LASER HOLOGRAPHIC MEASUREMENTS

I.1 Introduction

Conventional linear elastic fracture mechanics cannot explain fracture in concrete and mortar. Unlike traditional LEFM materials which show a constant fracture toughness, concrete and mortar toughen (show more resistance to fracture) as cracks propagate until an instability results and the structure fails. This increase in toughness is thought to occur because of many possible complex mechanisms which take place during fracture in concrete and mortar. These mechanisms include: formation of a zone of microcracking around the crack tip; crack bridging, where aggregate particles span the crack and act as ligaments to hold the crack together; and crack deflection, where the crack changes direction. All of these mechanisms require additional energy input into the system and may explain the apparent toughening of the material.

I.2 Cohesive Crack Models

Cohesive zone models based on the Dugdale-Barrenblatt approach of placing a closing pressure on the faces of a discrete crack (Fig. I.1A) could be used to account for the non-linear effects of the FPZ and aggregate interlock. Hillerborg, et. al.[1] proposed a cohesive model for cement based materials. This model assumes that the closing pressure is a function of the crack opening (w); Fig. I.1B). Jenq and Shah[2] proposed a model where K_I was not equal to zero (Fig. I.1C). Cook, Fairbanks, Lawn and Mai[3] also used a model where K_I was not equal to zero and which had a degree of crack length dependence (This model was for ceramic materials, but may be applicable to cement based materials; Fig. I.1D). It is assumed in the Cook model that the material has randomly spaced "ligaments" which cause the closing pressure. Short cracks intersect no ligaments so there is no closing pressure while long cracks intersect so many ligaments that a steady state closing pressure is used. Roelfstra and Wittmann[4] and Alvarado and Torrent[5] argued that the shape of the closing pressure vs. w curve was very important and affected the predicted post-peak branch of the load vs. crack mouth opening displacement (CMOD) curve. Roelfstra and Wittmann also suggested that different closing pressure vs. w curves were needed for concrete and mortar with different maximum aggregate sizes. Liaw, Jeang, Hawkins and Kobayashi[6] proposed closing pressure vs. w relationships based on concrete strengths.

I.3 Review of the Experimental Data

The crack profile data used during the course of this research was obtained by the use of laser holographic interferometry. A brief summary of the experimental method is presented here and further detail can be found in Reference 10.

A center notched plate specimen, made of mortar, was tested (Fig. I.2). The mortar had a ratio of cement/sand/water of 1/2.65/0.65 and the maximum particle size was 3mm (0.125 inch). The specimens were loaded in parallel with strain gaged steel bars to provide stable crack growth (Fig. I.3A).

At approximately 0.5 kN (100 pound) increments, the specimen was hologramed and holograms from two different load steps were combined using a technique called sandwich holography[7]. When the hologram is viewed, the

1

surface of the object is covered with fringes and the crack appears as a discontinuity in the fringe pattern (Fig. I.3B). If the crack is crossed, some fringe orders will be missing. The number of missing fringe orders can be found by tracing a line around the crack and determining the number of fringes crossed by the line. The opening of the crack is proportional to the fringe counts.

Miller, Shah and Bjelkhagen[8] showed that short cracks have profiles which are basically the same as LEFM profiles. Longer cracks have profiles which are much thinner than LEFM crack, suggesting that applying a closing pressure to the LEFM profile may provide the correct final profile (Fig. I.4).

I.4 Closing Pressures to be Studied

Four different closing pressures have been chosen for study. In choosing these closing pressures, consideration was given to both the similarities and differences between the experiments which produced these relationships and the holographic experiment which will be used here for comparison. In general, three things were considered: type of material used (i.e. maximum aggregate size, w/c ratio), type of specimen and method of crack width measurement. Figure I.5 is a summary of the closing pressure relationships studied and Table I.1 compares available properties.

The first is an exponential closing pressure proposed by Gopalaratanam and Shah[8]. This closing pressure was developed from tests of three different materials; a concrete, a mortar and cement paste.

The second relationship was a bilinear curve proposed by Roelfstra and Wittmann[5]. As was previously noted, Roelfstra and Wittmann thought that maximum aggregate size was an important parameter and they produced a series of bilinear curves for different types of concrete and mortar. The bilinear curve chosen for this study was a curve for a mortar which had the same maximum aggregate size as the mortar used in the holographic study.

A trilinear closing pressure proposed by Liaw, Jeang, Hawkins and Kobayashi[7]. This closing pressure was chosen for analysis because the crack line wedge loaded double cantilever beam specimen used by Liaw, et al., was very similar to half the center cracked plate used in the holographic study and because the closing pressure relationship uses strength of the concrete as a parameter.

The final closing pressure relationship studied was a linear relationship proposed by Cedolin, Iori, and Dei Poli[9]. The importance of the linear closing pressure (and the reason for its inclusion in this study) is that this is the only other published study the authors could find which used an optical laser method to measure crack opening.

I.5 Methodology of Analysis

The analysis in this study was performed by using a finite element program where the given closing pressure was applied to the crack faces. The resulting crack profile was then compared with holographically measured crack profiles. An iterative procedure is needed because the closing pressure depends on the unknown crack opening, w. If the closing pressure is too high, the calculated crack opening displacements become negative (overlap of crack faces). Special provisions have to be made in the finite element program to prevent overlapping.

I.6 Material Properties

In addition to the plate specimens, 50.8 mm X 101.6 mm (2 in X 4 in) cylinder specimens of the same mortar were tested in uniaxial compression at

2

comparable age. Two linear variable differential transducers (LVDTs) with a 50.8 mm (2 in) gage length were mounted on diametrically opposite sides to measure axial deformation. The initial tangent modulus was used during the analysis.

Measured tensile strength shows considerable scatter and there is a marked variation depending on the method used to determine tensile strength. Depending on the method used, tensile strength may vary from 7 to 14% of the compressive strength (f'_c)[10]. This scatter will affect the consistency of the model. In this study, tensile strength was assumed to be:

$$f'_t = 0.10f'_c$$

I.7 Analysis of the Closing Pressure Models for $K_I = 0$

The applied load P_a and $K_I = 0$ were specified and then, the crack length was calculated. This was done by applying the experimental load to the mesh and then propagating the crack 3 mm (1/8 in) at a time. At each increment of crack length the closing pressure was applied and a value of K_I calculated until a value of $K_I = 0$ was found.

For some closing pressures it was not possible to find a $K_I = 0$ crack length since K_I became either constant or began to increase (Fig. I.6). This occurred only at the peak load. In this case the minimum K_I was used for the $K_I = 0$ length, but these cases will be noted in the analysis.

Figure I.7 shows the predicted crack length for $K_I=0$ vs. measured crack length. Except for the trilinear closing pressure, all the closing pressures predict the correct crack length within the experimental accuracy (shown by the dashed lines). Therefore, accurate prediction of thee crack length is not restricted to a unique closing pressure.

A better evaluation of the different closing pressures results from comparing the experimental crack profiles vs. predicted crack profiles. In order to provide an objective comparison, an error definition is proposed:

$$error = \frac{\Sigma \ (w_{K0} - w_h)}{\Sigma w_h}$$

where: w_h = measured holographic crack opening at a node

w_{K0} = crack opening for $K_I = 0$ profile at the same node

The sum is taken over the number of finite element nodes along the crack face (spaced at 3mm apart). A positive error means the closing pressure was not large enough to close the LEFM crack profile down to the holographic profile while a negative error means the closing pressure was too strong and closed the LEFM crack profile down too much.

Figure I.8 shows the error for all the specimens tested. From figure I.8 it is apparent that comparable results were obtained for the cracks developed on specimens of same strength (i.e. same results for specimens tested on 1/30 and 1/31) which may indicate a strength dependance on the closing pressure. Also, note that with the bilinear closing pressure, short cracks are closed too much even though for the longer cracks there is good agreement between experimental and predicted results. This may indicate the use of less closing

3

pressure near the crack tip (most important for short cracks) while for longer cracks this closing pressure may be adequate. This is not surprising since it was previously shown that short cracks are nearly LEFM cracks and no closing pressure is required. In the other hand, the trilinear closing pressure shows a somewhat opposite behavior. For short cracks there is a relatively good match while for long cracks the closing pressure appears to be too strong.

I.8 Proposed Adjustments to the Bilinear Closing Pressure

Out of the four closing pressures examined, the bilinear closing pressure provided the "best" fit, although the fit was not very good. The next step seemed to be to see if the parameters of the bilinear curve could be logically adjusted to provide a better fit. Since the crack lengths and holographically measured crack openings are known, it is possible to calculate the required closing pressure distribution that exactly matches the experimental results. Figure I.9 shows some sample calculated closing pressure distributions.

Cook, et. al. [4] proposed that crack length dependence could be accounted for in the cohesive crack model by assuming that there is some initial distance over which the closing pressure does not act (see introduction). This agrees with figure I.4 that shows good agreement between experimental and LEFM crack profiles (no closing pressure) for short cracks. This model can be incorporated into this study by releasing the closing pressure from some of the nodes, i.e. making some nodes ahead of the original not tip traction free.

An objective procedure to obtain the best bilinear closing pressure for all the cracks analyzed was proposed. The penalty function f given by:

$$f = \Sigma \ error_i^2$$

where:

$error_i$ = relative error for load step i

was defined and a bilinear closing pressure defined by four parameters (f_t, f_1, w_1 and w_0; Fig. I.9) is considered. An algorithm was applied to minimize the penalty function for each specimen. The same algorithm was applied for various lengths of the traction free zone in front of the notch tip (as proposed be Cook) with the best results for a traction free zone of 8 mm (1/8 in). A proposed bilinear closing pressure, based on the optimization procedure is shown in figure I.9.

Table I.2 shows the results of the optimization precess. Even though only two different strengths were tested some conclusions can be made. There is a clear strength dependence on the stress parameters (f_t and f_1) while the crack opening parameters converged to the same solution regardless of the strength of the material. Also, note that for the specimens tested, the optimized value of f_t is about 10.5% of f'_c which agrees with previous experimental measurements of the tensile strength of concrete.

Figure I.10 shows the relative error plots for the proposed bilinear closing pressure and typical crack profile comparison. Note that there is a good prediction of the crack opening displacements although the crack lengths are over estimated including a segment close to the crack tip with either small or null predicted crack opening.

Jenq and Shah suggested that K_I did not need to be equal to 0. If the closing pressure is applied K_I corresponding to the experimentally observed crack length is calculated, an upper bound for each specimen is observed (Fig. I.11).

4

An upper bound is used because the holograms are made at discrete points during the loading and it is not possible to tell if the crack is just about to propagate, has just propagated or is somewhere in between. Figure I.12 shows the relative error plots and typical crack profiles corresponding to the upper bound value of K_I from figure I.11. Note that there is no significant effect on the results.

I.9 Discussion and Conclusions

This study clearly shows that the cohesive crack model can correctly predict crack behavior but that the assumption that the closing pressure depends only on the crack opening, w, may not be correct. The results show that strength, maximum particle size, and crack length are also important parameters. The assumption that $K_I = 0$ seems to be acceptable as long as the actual $K_I = 0$ crack length is calculated and not assumed. In addition, it is very important to note that the values of modulus and tensile strength greatly affect the model. Due to the limited amount of accurate data on crack lengths and crack opening displacements, the authors cannot yet propose exact modifications to the closing pressure functions, although the Cook, et. al.[4] model seems to be a good start on including crack length effects into the cohesive crack model. The authors hope that as more holographic experiments are performed on different mixes and specimens, a clearer picture of the necessary changes to the cohesive zone model may emerge.

This research did not address the question of making the area under the closing pressure curve equal the fracture energy, G_f. While the fracture energy is an important parameter, it seems that there is no agreed upon value or function for G_f. Values of G_f can be found in literature to justify almost any closing pressure. Therefore, more work needs to be done on defining G_f for concrete before it will be a useful parameter for closing pressures.

5

TABLE I.1

COMPARISON OF CONCRETE PROPERTIES

REFERENCE/CLOSING PRESSURE	MAXIMUM AGGREGATE (mm)	f'_c MPa	f'_t MPa	w/c
Cedolin (Linear)	8	41.4	3.2	.5
Roelfstra(Bilinear)	3	N/A	4.7	.58
Jeang (Trilinear)[*]	6-12	27-62	2.3-3.5[+]	N/A
Gopalaratanam (Exp)[*]	0-10	33-47	N/A	.4-.6
Miller (Holographic)	3	28 & 47	N/A	.6

[*] Multiple mixes used to find closing pressure

[+] From formula $f'_t = .45\sqrt{f'_c}$ fit to experimental data

TABLE I.2

OPTIMIZED BILINEAR CLOSING PRESSURE

TEST DATE	f'_c (MPa)	f_t (MPa)	f_1 (MPa)	w_1 (micron)	w_0 (micron)
8	28	3.13	1.45	3.81	73.66
30	47	4.47	2.16	3.81	67.56
31	47	4.91	1.75	3.82	69.60

Part II.   MEASUREMENT OF STRAIN FIELD IN FRACTURE PROCESS ZONE OF MORTAR

II.1 Introduction

The study presented in part I shows that the cohesive crack model approach can be used to predict both crack extension and crack opening displacements. However, the fracture process in concrete is not limited to discrete macrocracks. Several phenomenon have been associated to the so called fracture process zone (FPZ) such as microcracking around the crack tip and strain softening. A key to a better understanding of fracture of concrete is the accurate observation of the fracture process zone.

The first observation of this kind was made by Cedolin, Dei Poli and Iori. They used laser moiré interferometry for wide field measurements in specimen under tension. White light moiré interferometry was also used by Du, Kobayashi and Hawkins[11] to measure crack opening displacement along the fracture process zone (FPZ) for concrete specimens under three point bending. Regnault and Bruhwiler[12] used moiré holographic interferometry to measure strain field on wedge splitting test specimens and concluded that the model based on the exact knowledge of traction free crack tip location does not describe the material behavior in a realistic way. Raiss, Dougill and Newman[13] also used laser moiré interferometry to measure strain field on direct tension specimens.

In the technique described in this report, three simultaneous holograms were taken by illuminating the specimen from three different directions. In addition, digital image analysis techniques were developed to accurately evaluate wide field in plane deformation. The results of the strain field calculation obtained using this newly developed technique for mortar center notched plate specimens are discussed.

II.2 Experimental Program

Center notched mortar plate specimens were used (Fig. II.1). 3 in x 6 in (76 mm x 152 mm) cylinders were also cast in order to determine the compressive strength and initial modulus of elasticity. Two cylinders with 1/2 in (13 mm) strain gages were tested in a closed loop testing system under strain control the day after the center notched specimen test was performed.

Holographic interferometry was used to measure crack opening displacements and the strain field on a 2 in x 3 in (51 mm x 76 mm) area in front of each notch (i.e., top and bottom; Fig. II.1).

II.3 Holographic Interferometry Test

Each interference pattern represents the component of the displacements onto the sensitivity vector k[7]. In the optical set-up shown in figure II.2 all the optical paths are on a plane of constant height (y=constant). Therefore, the sensitivity of the optical system to vertical displacements is small. In addition, the loading configuration restrains displacements in the y direction. Thus, two displacement components are sufficient to describe to motion of any point on the specimen, namely the in plane component (x) and the out of plane component (z). In order to obtain a two dimensional displacement field (in plane and out of plane), in principle, two interferograms are required. However, since there is no sign associated to the fringe counts a third interferogram is necessary. Figure II.3 is an schematic view of the optical set-up with three illumination directions (R,L and C) used for this study.

For each load step a different sandwich hologram[14] is recorded from each illumination direction (holograms R,L and C). Due to the incremental nature of the holographic measurements, it is necessary to make a series of sandwich holograms at continuous load levels. If a load increment is not recorded none of the future deformation states can be computed.

II.4 Enhancement of Holographic Interferograms by Image Analysis

The holographic interferograms were acquired into a Tracor Northern image analysis system using a slow scan high resolution COHU camera. A schematic arrangement for reconstruction of the holographic images and acquisition into the image analysis system is show in figure II.3. The acquired image (grey image) contains a range of intensities (0-255) representing different grey levels.

The bright and dark bands of the holographic fringes can be represented as a binary image. In a binary image the pixel intensities assume only two values, ON (or 1) for perfect white and OFF (or 0) for perfect black. Due to variations of intensity of the object beam throughout the surface of the object, it is possible that a bright band at a section of the image has a lower intensity magnitude than the dark bands at other segments of the image. Standard methods of image processing such as thresholding from a certain pixel intensity are thus inapplicable. This situation is represented by the plot in figure II.4a which shows the intensity variations along a cross section of a holographic grey image.

If I_1 and I_2 are the intensities of the individual images in a sandwich hologram, the intensity of the resulting interference pattern is:

$$I = (I_1 + I_2) + 2(I_1 I_2)^{1/2} \cos \Delta\phi \qquad (1)$$

From this equation it is apparent that the intensity value of any pixel can be separated into two terms. One is the average intensity of the image $(I_1 + I_2)$, and the second depends on the phase difference between the two wave fronts $(\Delta\phi)$. The separation of this two terms can be achieved through the use of the image analysis system.

Assume that the grey image of the sandwich holography interferogram is represented as IMAGE_1 where as IMAGE_2 is the average of the independent wave fronts acquired separately (Fig. II.4a). Subtraction of IMAGE_2 from IMAGE_1 results in the isolation of the interferometric effect, represented as IMAGE_3 in figure II.4b. Since negative values are not allowed as meaningful intensity values, IMAGE_3 results in zero for all the pixels on dark bands. The bright bands retain a positive magnitude. By selecting all positive values a binary image is created (Fig. II.4c).

II.5 Fringe Count

IMAGE_3 is the enhanced interferometric image in which the intensity value is zero for dark bands and one for bright bands. Further image processing allows to assign intensity values to each fringe corresponding to the same fringe order.

Figure II.5 shows a fully processed interferogram in which same intensity values correspond to same fringe orders. Note that there is a different intensity level for each half a fringe (i.e., different intensity for dark and bright bands). The fringe count between any two points can now be easily

8

obtained by computing half the difference of the corresponding intensity levels (e.g., fringe count between A and B in figure II.5 is $(90 - 65)/2 = 12.5$).

Even though the use of the image analysis system results in very fast fringe counts, speed is not the main advantage of this technique. The isolation of the interferometric effect on the holographic images and the binarization process result in accurate and objective fringe counts. The gradual change in intensity from a dark to a bright band make it very difficult to obtain consistent fringe counts when conventional (by hand) methods are used.

II.6 Evaluation of Holograms

The holodiagram[15] shown in figure II.6 is a simple geometrical tool for computation of displacements based on interferometric readings. In figure II.6 the distance I-P-O from illumination point to object to observation point (usually taken as the position of the holographic plate) remains constant if the object (P) moves along ellipse E_1 (or an ellipsoid in the most general three dimensional case) with foci at illumination and observation points. Now, define ellipse E_2 such that the distance I-P-O increases by $\lambda/2$ (180° phase difference). An interferogram of the object that moved from any point on ellipse E_1 to any point on ellipse E_2 will show a dark band (half a fringe) due to destructive interference of the wave fronts. In general, the number of fringes is proportional to the increase (or decrease) of the distance I-P-O.

From figure II.6 it is apparent that there are an infinite number of possible displacement vectors which result on the same fringe count. The number of possible displacement vectors is reduced to four by using two holograms with different illumination points and fringe counts n_1 and n_2 (inset of figure II.6). Using a fringe count from a third hologram, it can be determined if n_1 and n_2 have the same or opposite sign.

II.7 Crack Profiles.

For the computation of the crack opening displacements (COD) the modified Nelson and McCrickerd [16][8] method was used. This method assumes the out of plane motion to be negligible (i.e. COD is the main component of the displacement) and that displacements are small. Since the direction of motion is assumed, one hologram is sufficient. This was described in part I.

An alternative solution is to assume a two dimensional displacement solution. The displacement is computed as the difference in position of the intersection of the ellipses from two illumination directions. The holographic fringe counts can be combined in three possible ways (R and L, R and C, C and L). As mentioned before, the third fringe count is necessary to select the correct value among the four possible displacement solutions for each combination. Figure II.7 shows a crack profile computed using all three combinations. Note that there is an improvement in the scatter on the COD calculations with respect to the Nelson and McCrickerd results. Also, note that taking into account the out of plane contribution to the fringe counts results in smaller CODs even for an experimental set-up designed for mode I crack propagation. This means that there exist a measurable component of the crack face displacement in the out of plane direction (mode II) which can explain the presence of compressive strain behind the crack tip as reported by Bruhwiler. The doted line in figure II.7 represents the crack sliding displacement (CSD) in the XZ plane.

II.8 Strain Fields.

9

Fringe counts relative to the left face of the crack, or the symmetry line for point beyond the crack tip, were taken at every point on a 3 in x 3 in (76 mm x 76 mm) grid every 1/8 in (3 mm) for all three holographic images (R,L and C). A computer program was used to calculate the relative displacement of every point relative to the left face of the crack by locating the intersection point of the holodiagrams corresponding to each illumination direction. The strain field was obtained by differentiation. Figures II.8 show the strain field (ϵ_{xx}) around the bottom crack for crack lengths of 1.375 in (35 mm), 1.875 in (48 mm) and 2.25 in (57 mm), corresponding to 1324 lb (6.0 KN), 1461 lb (6.6 KN) and 1601 lb (7.2 KN) of applied load. It is important to notice that during the experimental program, before any holograms were made, the specimens were placed under a 800 lb (3.6 KN) preload. This preload is necessary to keep the specimen optically stable. The strain fields shown in figures II.8 include only the measured additional strain after the initial preload state.

In general, a high strain (>100$\mu\epsilon$) region can be found around and in front of the crack tip with a maximum value of approximately 300 $\mu\epsilon$. Behind the crack tip there is a zone of negative strain which suggests relaxation of tensile strain with respect to the initial preload stage.

II. 9 Definition of the Fracture Process Zone

The zone where the measured strain values exceed 100 $\mu\epsilon$ (limit to define nonlinearity) are shown in figures II.9 for three crack lengths. Also shown in the figure are the zones behind the crack tip where tensile strain was detected. Note that the end of these zones correspond approximately to the tensile strain value of zero. There appears to be a traction free zone of approximately 0.25 in front of the original notch tip regardless of the crack length and COD indicated by w_c in figures II.9). This agrees with the model suggested by Cook, et. al.[3]

An alternate approach to define the FPZ is to find the deviations from the linear elastic solution. The specimen was analyzed using a finite element program. In order to make a valid comparison with the experimental results, figures II.10 show the LEFM strain distribution corresponding to the difference between the given load level and the initial preload. Note that the strain levels surrounding the crack tip exceed those from the holographic measurements (Fig. II.8)

Behind the crack tip the LEFM solution shows sharp unloading. At 1601 lb the strain drops from 500 $\mu\epsilon$ at the crack tip to zero within 1/8 in behind the crack tip. In contrast, the observed strain relaxation shown on figure II.8 follows a gradual descent.

In figures II.11, the differences in strain fields between the LEFM solution and the experimentally measured values are shown. It is arbitrarily assumed that the differences are significant when they exceed the strain value of 60 $\mu\epsilon$. The zones marked A in figure II.11 are the regions where the LEFM solution predicts tensile strain values 60 $\mu\epsilon$ higher than those measured holographically. Note that this zone remains essentially constant regardless of crack length. Since this zone is relatively small and does not change with crack length a model based on modified LEFM may be a possible approach. This is discussed in the next section. The zones B, with negative values, typically found behind the crack tip show that the relaxation of the observed strain is 60 $\mu\epsilon$ less than that in the elastic solution. Zones B can be defined as the wake of the fracture process zone (WFPZ) and they enclose the area where extensive microcracking has been developed and tensile forces are still

transmitted through the crack. Behind this zone, the fracture process approaches a traction free condition.

II.10 Closing Pressure Analysis

The cohesive type of model with a bilinear closing pressure described in part I was used to simulate the effect of the fracture process zone. To examine whether such a model can accurately predict the measured strain field, the same finite element program with singular elements was used. The predicted crack profiles in figure II.12 show a good correlation with the experimental values.

Figures II.13 show the difference in strain field predicted using the closing pressure approach and the observed values. Note that there is a good correlation of the results and the zones with significant deviation from the experimental results are practically eliminated ($\pm$ 60 $\mu\epsilon$).

II.11 Conclusions

a. Sandwich hologram interferometry with multiple sensitivity vectors can be used to measure crack opening displacements and strain fields in mortar specimens under tensile stress. When holographic interferometry is used to measure Mode I crack opening displacements the effect of out plane motion should be taken into account.

b. Digital image analysis facility provided a faster, more consistent and more accurate method of fringe count than the manual method.

c. There is a region of high tensile strain that moves with the tip of the propagating crack. The material behind the crack tip experiences strain relaxation. However, the gradual nature of the strain relaxation demonstrates the existence of tensile force transmitted through the crack faces.

d. Zones of nonlinear behavior can be located by computing strain field deviations form the linear elastic solution.

e. A bilinear closing pressure vs. COD cohesive crack model has been proposed to predict both crack profiles and strain field, fully characterizing the material behavior.

11

Part III.   A STUDY OF MIXED MODE CRACK PROPAGATION IN MORTAR USING HOLOGRAPHIC
           INTERFEROMETRY

III.1 Introduction

In a mode I pure tensile situation described in parts I and II, the application of a cohesive crack model is beginning to be understood[17][18]. Most practical situations however involve a combined presence of tensile and shear cracking. This creates a mixed mode condition involving both mode I and mode III stress intensity factors. It is important to study if the theoretical developments of mode I condition can be extended in principle to a mixed mode situation. Only a limited number of studies have been conducted on mixed mode loading of concrete and other quasi-brittle materials [19][20][21][22][23][24]. Most of this work is under tensile shear condition. There is a lack of information about compression shear crack initiation which is being addressed in this report. It is also important to study the phenomena involved when the relative magnitude of the mode I and mode III stress intensity values are varied at the crack tip creating different types of mixed mode situations. This is particularly important because of the coupling between the shear and tensile openings of crack in such materials where the aggregate interlocking and crack surface irregularities could affect the final crack profile.

III.2 Theoretical Background

The theoretical considerations are based on an infinite plate under uniaxial compressive stress in the far field (Fig. III.1). The plate has an existing crack length at an angle β to the direction of the applied load. The crack can be considered to be subjected to the far field stress condition shown in the figure III.1 where:

$$\sigma_y = -\sigma \sin\beta, \qquad \sigma_x = -\sigma \cos\beta, \qquad \tau_{xy} = -\sigma \sin\beta \cos\beta$$

where for compressive stress $\sigma > 0$ the mode I and mode III stress intensity factors at the crack-tip are given by:

$$K_I = -\sigma \sqrt{\pi a} \sin^2\beta, \qquad K_{II} = -\sigma \sqrt{\pi a} \sin\beta \cos\beta \quad (\sigma > 0)$$

It is hence possible to vary the ratio of K_I/K_{II} by varying the inclination angle β. Negative value of K_I implies closure of the original notch. Negative value of K_{II} does not have any such significance but affects the direction of crack propagation. Crack initiation of the inclined crack under compression is associated with closure of the original notch. Cracks are initiated under a combination of compression and shear. Note that once the crack initiates and propagates, the propagating crack is under tension and shear.

The equation above provide an insight into the nature of the problem but are valid only for an infinite plate. Due to the finite size of the specimen and the gradual curving of the propagating crack, is was essential to conduct an FEM analysis of this problem at different stages of crack propagation.

III.3 Finite Element Analysis

In order to study the Stress Intensity Factors (SIFs) and displacements of the actually tested specimens a FEM program with quarter point singular elements was used[25]. Figure III.2 shows a typical FEM mesh used during this study. Note the triangular elements (singular elements) at the notch tips. As

the crack propagates it was necessary to modify the FEM mesh accordingly. This was done by using an interactive code FRANC which has automatic remeshing capabilities. In the experimental program four types of specimens were testes which were of the same dimensions except for the initial notch inclination angles β. Four different values of β were used (18°, 36°, 54° and 72°). A program was written to generate the four types of input meshes corresponding to the four inclination angles.

Figure III.3 compares the solutions obtained from the FEM analysis to the solution from the infinite plate analysis discussed above and the solution for finite geometry obtained by Murakami[26]. The plotted data are values of K_I at the tip of the original notch of inclination β when the applied compressive stress is equal to the stress at which the crack starts to propagate. The figure shows that the values obtained from the FEM solution are very close to Murakami's solutions. The infinite plate solutions are found to give somewhat lower results.

III.4 Experimental Program

Specimens were made with 3:1:0.6 mixture of sand, type I cement and water. The central portion of the specimen was 8" X 6" X 3" (20.3 X 15.2 X 7.6 cm). Two separate end blocks were cast for each end and measured 1.5" X 6" X 3" (3.8 X 15.2 X 7.6 cm; Fig. III.1). The end blocks were made to reduce the effect of the end friction from the loading platen. It has been observed that this simple method is the best way to ensure an uniform uniaxial compression in the central portion of the specimen[27]. The specimens were cast in plexiglass molds. The end pieces were cast simultaneously with the center piece by placing 1/16" (0.16 cm) plexiglass separators in the molds. The notch was 2" X 0.078" (5.08 X 0.2 cm) and was cast by placing a steel blade in the mold while casting. The blade was attached to an aluminum frame which was fixed to the side of the mold. The blade was attached by a screw and a nut arrangement which made it possible to change the angle of the plate and cast all four types of specimens with the same set of molds. The molds were oiled and the plates were greased prior to pouring the mixture. The blade were removed four hours after casting when the mortar had set not yet harden. Once the mortar hardens it is difficult to remove the blades without damaging the specimen. The specimens were demolded 24 hours after casting and cured in water at room temperature thereafter. They were tested about 60 days after casting.

The specimens were tested in compression under 120 Kip MTS loading machine. They were capped with quick setting cement and the surfaces between the end blocks and the center block were greased to ensure an uniform load distribution. The loading was displacement controlled by using two Linear Variable Differential Transducer (LVDT) which monitored the actual deformations.

In order to measure the opening and sliding of the crack close to the initial notch tip, two clip gages specially design at our laboratory were used (Fig. III.4). Three specimens of each group (each angle) were tested. Clip gages were not used on the first specimen of each group because the crack propagation directions were not known and because the investigators were apprehensive of unstable failure damaging the gages. The clip gages were mounted on aluminum mounts as shown in figure III.4. The concrete surface was first polished and the mounts were fixed with super glue adhesive. Small amount of epoxy was used on the side of the mounts to provide additional strength. The finite dimension of the aluminum mounts (about 1/4" or 0.64 cm) and the epoxy makes it to average the crack opening and sliding over a finite distance.

Hence, the clip gages effectively measure the crack opening and sliding at a distance of about 1/4" from the notch tip. The data from the LVDTs, the Load Cell and the clip gages were automatically monitored by a four channel Nicolet 4094 digital oscilloscope.

III.5 Holographic Interferometry

The experimental focus of this report was on developing an adequate experimental technique for studying the phenomena described above. Since the crack propagation in the experiments conducted were at different places on the specimens and the crack path was inclined and not known a priori it was necessary to have a technique with full field detection capability. It is necessary to have a technique with the highest sensitivity (fraction of a micrometer, comparable to the intercristal space in mortar). Due to the nature of the material and the size of the specimens, the technique should be noninvasive and noncontacting so as to have the least influence on the specimen tested. Holographic Interferometry (HI) was adopted as the technique that best satisfied all the criteria described above. This method which is typically used for visual inspection of cracking, delamination and for out of plane displacement measurement was used in this experiment to simultaneously measuring both the in plane shear and tensile crack openings by using an innovative technique.

Two specimen of each group were tested by an automated holographic system (Holographic 6000). It was possible to make a large number of holograms by this system and observe the propagation of crack at different stages of loading[28]. Crack propagation starts from the notch tip and the crack curves to the direction parallel to the direction of applied loading (Fig. III.5). The holograms of some typical specimens are shown in figure III.6. Crack propagation is evident as discontinuities in the fringe pattern.

A specimen of each group was tested by an innovative approach based on quantitative measurement techniques using holography[29]. The fringes in HI are caused by the displacements on the object surface. Each fringe corresponds to the component of the displacement along the sensitivity vector. The Sensitivity Vector (S) for any point on the object is the bisector of the observation direction (OQ) and the illumination direction (IQ) (Fig. III.7). Hence, a single observation gives only one displacement component. In order to find the three independent displacement components of a specimen it is necessary to use three different illumination or observation directions. Typically this is restricted by the cost of additional optics and the trouble involved in making three times as many holograms. It is also difficult at times to avoid rigid body motion in between making the three holograms for each loading stage. In figure III.7 if the displacement δ of the point Q has a component along S equal to QC, the path length of the beam at that point changes by the amount (QA+QB).

$$QA + QB = 2 \ QC \ \cos\theta \qquad \text{and the component} \ QC = \delta \ \cos\psi$$

So the total path change is equal to: $2\delta \ \cos\theta \ \cos\psi$
The path length change contributing to a fringe (dark or light band) is $\lambda/2$ where λ is the wave length of the He Ne laser used in this work (.63 micrometers). Hence, a fringe count of n corresponds to a displacement of:

$$\delta = \frac{n\lambda}{4 \cos\theta \, \cos\psi}$$

It is possible to count fringe to an accuracy of 1/2 fringe (from the middle of a dark or light fringe to the edge of the same fringe) and in our experiment, θ was approximately equal to 25°. The accuracy of the set-up to measure displacement along the sensitivity vector is limited to:

$$accuracy = \frac{(1/2)\,(0.63)}{4 \cos 30} = 0.09 \text{ micrometers}$$

The method adopted here gets around these draw backs without any significant sacrifice in accuracy. This is achieved by using a single 4" X 5" (10.2 X 12.7 cm) holographic plate placed very close to the specimen surface (Fig. III.8). This makes each point on the object surface subtend a large angle on the holographic plate. Effectively, it is now possible to look at the object through four corners of the plate. The observed fringe pattern is different from the four corners due to the differences in observation directions. By counting the fringe patterns from the four corners of the same plate we have a set of four equation involving the three unknown displacement components and the four different sensitivity vectors. The accuracy of this set-up is demonstrated in figure III.9. If the plate is placed close to the specimen, A and B era the two points on the plate through which observation of the fringes are made. S' and S" are the two sensitivity vectors corresponding to the observation directions A and B. If the in plane displacement of point Q is δ, its components along S' and S" are δ dot S' and δ dot S" (dot product). δ is evaluated from the difference in fringe patterns as observed from A and B. As in figure III.8, the displacement δ caused a path length change of $2\delta \cos\theta'$ $\cos\psi'$ and $2\delta \cos\theta"$ $\cos\psi"$ respectively to the observation points A and B respectively. ψ' and $\psi"$ are the angles between the in plane displacement and the sensitivity vectors. If the fringe counts at points A and B were n_1 and n_2 respectively, then:

$$n_1 = \frac{4 \delta \cos\theta' \, \cos\psi'}{\lambda} \quad \text{and} \quad n_2 = \frac{4 \delta \cos\theta" \, \cos\psi"}{\lambda}$$

the difference in fringe counts from A and B is:

$$(n_1 - n_2) = 4\delta (\cos\theta' \, \cos\psi' - \cos\theta" \, \cos\psi") / \lambda$$

A computer program was developed which could calculate the sensitivity vectors when the coordinates of the optics were input. The fringe counts were input into the program which solved the four equations in the least square sense to find three unknown displacement components. The in plane displacement components (crack opening and sliding profiles) were then evaluated by the program. It needs to be mentioned that placing the holographic plate in front of the specimen makes the set-up more sensitive to the out of plane direction than in the in plane direction. It is necessary to place the plate as close to

the specimen as possible to increase the in plane sensitivity. Proximity of the plate to the specimen is restricted by other considerations such as the coherence length of the laser, ratio of beam intensities (reference beam:object beam), etc. Despite the typically higher out of plane sensitivity of HI, the out of plane motions computed for the test specimens were much smaller than the crack opening and sliding displacements.

III.6 Experimental Results
The loads at different lengths of crack propagation were noted while crack extensions were observed by HI. A FEM study was done to find to find the SIFs and crack opening and sliding displacements corresponding to unit load at 1/2", 1", 1.5" and 2" crack extensions. The actual experimentally observed crack was analyzed in the FEM program where the gradual curvature of the crack was incorporated by a series of linear segments. The FEM analysis results where multiplied by experimentally observed crack propagation loads to get the results plotted in figures III.10 and III.11. The critical values of K_I (or K_{Ic}) at which cracks propagated is seen to vary widely. There is also a large discrepancy in the crack profiles shown in figure III.11. While for the 36° specimen the crack openings were mode than that predicted by FEM analysis, those for the 72° specimen were less. This was supposed to have been due to the traction and dilatancy caused by intergranular friction, ligament connection, etc. It was presumed that while the aggregate interlock prevented opening of the crack for the 72° specimen, sliding induced additional opening (dilatancy) in the 36° specimens.

III.7 Cohesive Crack Model
In order to account for the phenomena observed in figure III.10 and III.11 an analysis based on the model described in part I was used. The closing and sliding tractions were unknown in the absence of any adequate model and sufficient experimental evidence of mixed mode fracture behavior of mortar cracks. These tractions were obtained by applying unit opening and closing forces at intermediate points on the crack and finding the displacement profiles along the crack due to that unit force. If four points along the crack are considered, this results in a 8 by 8 matrix M where:

$$[L]_{1x8}[M]_{8x8} = [D]$$

D is obtained from the difference between FEM and HI displacements (Fig. III.11). L is obtained from the solution of the equation above. So L was obtained as the necessary traction forces on the crack faces which could explain experimentally observed displacements. The values of K_{Ic} were corrected for the values of L to give the corrected values shown in figure III.12. It can be observed that the values of K_{Ic} (corrected) are within a reasonably narrow band showing the possible applicability of a LEFM based criterion.

III.8 Conclusions
1. Holographic interferometry was found to be an excellent technique to study real time crack propagation with high sensitivity.
2. A single plate HI method can retain the accuracy of HI while measuring in plane displacements. This method eliminates lot of the expenditure and labor involved in multiple beam HI and can evaluate full field 3-D displacement field with a sensitivity of about 0.2 micrometers.

16

3.   A FEM program based on the Maximum Hoop Stress (MHS) criteria can predict the path of crack propagation in mortar under compression-shear loading with reasonable accuracy.

4.   The MHS criterion can not predict crack propagation loads due to the complexity involving interface tractions. The effects of these tractions have to be accurately modeled and considered if a LEFM based crack propagation criterion is to be postulated.

5.   An analysis involving the interface tractions contributed by a aggregate interlock, ligament connection and dilatation holds promise as a means of modeling mixed mode fracture behavior.

REFERENCES

1.   Hillerborg, A., Modeer, M. and Petersson, P. E., "Analysis of a Crack Formation and Growth in Concrete by Means of Fracture Mechanics and Finite Elements," Cement and Concrete Research, Vol. 6, No. 6, pp 773-782, 1977.

2.   Jenq, Y. S. and Shah, S. P., "A Fracture Toughness Criterion for Concrete," Engineering Fracture Mechanics, Vol. 21, No. 5, pp. 1055-1069, 1985.

3.   Cook, R. F., Fairbanks, C. J., Lawn, B. R., and Mai, Y-W., "Crack Resistance by Interfacial Bridging: Its Role in Determining Strength Characteristics," Journal of Materials Research, Vol. 2, No. 3, pp 345-356, 1987.

4.   Roelfstra, R. E. and Wittmann, F. H., "A Numerical Method to Link Strain Softening with Fracture in Concrete," Fracture Toughness and Fracture Energy in Concrete, F. H. Wittmann, ed. Elsevier Science Publishers, B. V., Amsterdam, 1986.

5.   Alvarado, A. M., and Torrent, R. J., "The Effect of the Shape of the Strain-Softening Diagram on the Bearing Capacity of Concrete Beams," Materials and Structures, Vol. 20, pp. 448-454, 1987.

6.   Jeang, F. L. and Hawkins, N. M., Nonlinear Analysis of Concrete Fracture, Structures and Mechanics Report, Department of Civil Engineering, University of Washington, Seattle, WA, 1985.

7.   Abramson, N., The Making and Evaluation of Holograms, Academic Press, 1981.

8.   Miller, R. A., Shah, S. P., and Bjelkhagen, H. I., "Crack Profiles in Mortar Measured by Holographic Interferometry," Experimental Mechanics, Vol. 28, No. 4, pp. 388- 394, 1988.

9.   Cedolin, L., Dei Poli, S. and Iori, I., "Tensile Behavior of Concrete," Journal of Engineering Mechanics, ASCE, Vol. 113, No. 3, pp. 431-449, Mar. 1987.

10. Mindess, S. and Young, J. F., Concrete, Prentice Hall, Englewood Cliffs, NJ, p. 400, 1981.

11. Du, J.J., Kobayashi, A.S. and Hawkins, N.M., "Fracture Process Zone of a Concrete Fracture Specimen," SEM/RILEM Int. Conference on Fracture of Concrete and Rock, Houston, Proceedings, edited by S.P. Shah and S.E. Swarts, 280-286 (1987).

12. Regnault, Ph. and Bruhwiler, E., "Holographic Interferometry for the Determination of Fracture Process Zone in Concrete," International Conference on Fracture and Damage of Concrete and Rock, Vienna, Jul. 1988.

13. Raiss, M.E., Dougill, J.W. and Newman, J.B., "Observation of the Development of Fracture Process zones in Concrete," pp. 243-253 _Fracture of Concrete and Rock_, Editors: Shah, Swarts and Barr, Elsevier Science Publishers, 1989.

14. Abramson, N., "Sandwich Hologram Interferometry: A New Dimension in Holographic Comparison,"Applied Optics, Vol. 13, pp 1143-1147, 1974.

15. Abramson, N., "The Holodiagram: A Practical Device for Making and Evaluating Holograms," Applied Optics Vol 8, pp. 1235-1240, 1969.

16. Nelson, D.V. and McCrickerd, J.T., "Residual Stress Determination Through Combined use of Holographic Interferometry and Blind Hole Drilling," Experimental Mechanics, Vol. 26, No. 4, pp 379-386, Dec. 1986.

17. "_SEM-RILEM Int. Conference on Fracture of Concrete and Rock_", Houston, TX, 1987, Ed. S.P. Shah and S.E. Swarts

18. Bazant, Z.P. and Cedolin, L, "Fracture Mechanics of Reinforced Concrete," ASCE J. of EMD, 106, 1980.

19. Bazant, Z.P. and Pfeiffer, P.A. "Shear Fracture Tests in Concrete," Materials and Structures, RILEM, 19, 110, 1986.

20. Swarts, S.E., Lu,L.W. and Tang, L.D. "Mixed-mode Fracture Toughness Testing of Concrete Beams in Three-Point-Bending," Kansas State University, 1987.

21. Desay, P. "Fracture of Concrete in Compression," Materiaux et Constructions, 10, 57, 1987.

22. Glucklich, J. "Fracture of Plain Concrete," ASCE J. of EMD, 1963

23. Nemat-Nasser, S. and Horii, H. "Compression-induced Nonplanar Crack Extension with Application to Splitting, Exfoliation and Rockburst," J. of Geophys. Rec., 87, 1982.

24. Tirosh, J. and Catz, E. "Mixed Mode Fracture Angle and Fracture Locus of Materials Subjected to Compressive Loading," Eng. Fracture Mechanics, 14, 1981

25. Wawrzynek, P.A. "interactive Finite Element Analysis of Fracture Processes: An Integrated Approach," Cornell University Structural Eng. Rep. 87-1, Supervised by A. Ingraffea.

26. Murakami, Y. "Stress Intensity Factors Handbook," Pergamon Press, New York, 1987.

27. Shah, S.P. and Sankar, R. "Internal Cracking and Strain Softening Response of Concrete Under Uniaxial Compression," ACI Materials J., 84, No. 3, 1987.

28. Maji, A.K. and Shah, S.P. "Application of Acoustic Emission and Laser Holography to Study Microfracture of Concrete," ACI SP-112, Nondestructive Testing, 1989

29. Pryputniewiez, R.J. "Holographic Application of Rigid Body Motions and Application to the Method to Orthodontics," Applied Optics, 18, 1977.

Fig. I.2.   Center Notched Plate Specimen.

strain-gaged steel bars

loading hole

loading device

P

P

y

x

z

Fig. I.3.   (A) Loading Arrangement, (B) Typical Holographic Interferogram.

CRACK OPENING DISPLACEMENT (in × 10⁻⁵)

CRACK LENGTH, a (in)

CRACK PROFILE
TEST DATE 1/30/87
TOP CRACK
f'_c = 47.5 MPa (6890 psi)
E_c = 28300 MPa (4.1×10⁶ psi)

LOAD = 7898 N

LOAD = 4793 N

△△△△△ MEASURED HOLOGRAPHIC
——— SMOOTHED HOLOGRAPHIC
– – – LEFM

CRACK LENGTH, a (mm)

CRACK OPENING DISPLACEMENT (microns)

Fig. I.4.   Comparison of LEFM Crack Profiles with Holographically Measured
Crack Profiles.

Fig. I.5.   Comparison of Closing Pressures.

Fig. I.6. K_I vs. Crack Length for Various Load Levels.

PREDICTED CRACK LENGTH, inches

MEASURED CRACK LENGTH, inches

PREDICTED VS. MEASURED
CRACK LENGTH
f'_c = 28.3 MPa (4100 psi)
TEST DATE 1/8 — BOTTOM CRACK

○○○○○ LINEAR
□□□□□ BILINEAR
△△△△△ TRILINEAR
◇◇◇◇◇ EXPONENTIAL

PREDICTED CRACK LENGTH, mm

MEASURED CRACK LENGTH, mm

Fig. I.7.   Measured Crack Length vs. Predicted Crack Length for K_I=0.

Fig. I.8. Crack Profile Comparison for $K_I = 0$.

Fig. I.9. Closing Pressures Calculated from Known Crack Profiles and the Proposed Bilinear Closing Pressure.
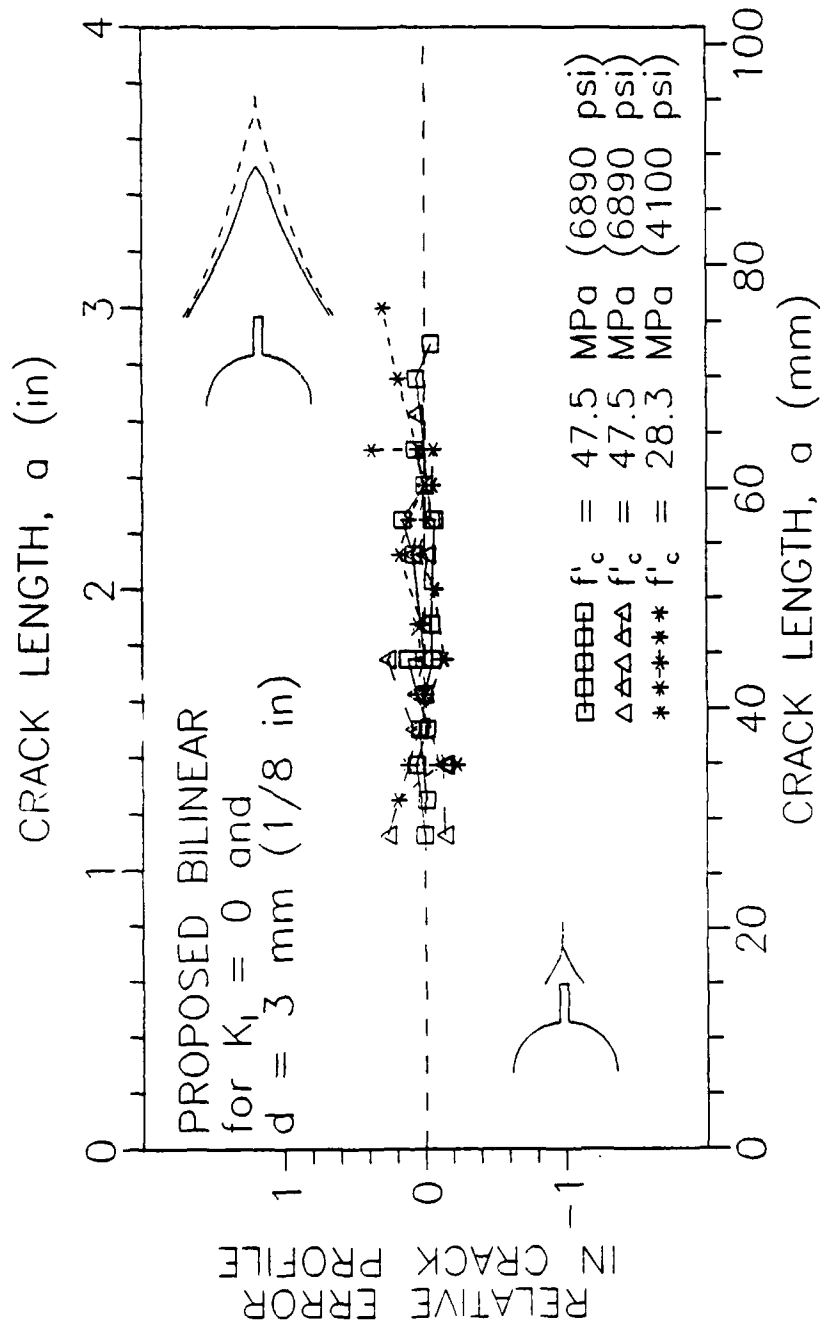
Fig. I.10. Crack Profile Comparison for Proposed Closing Pressure and $K_I = 0$.
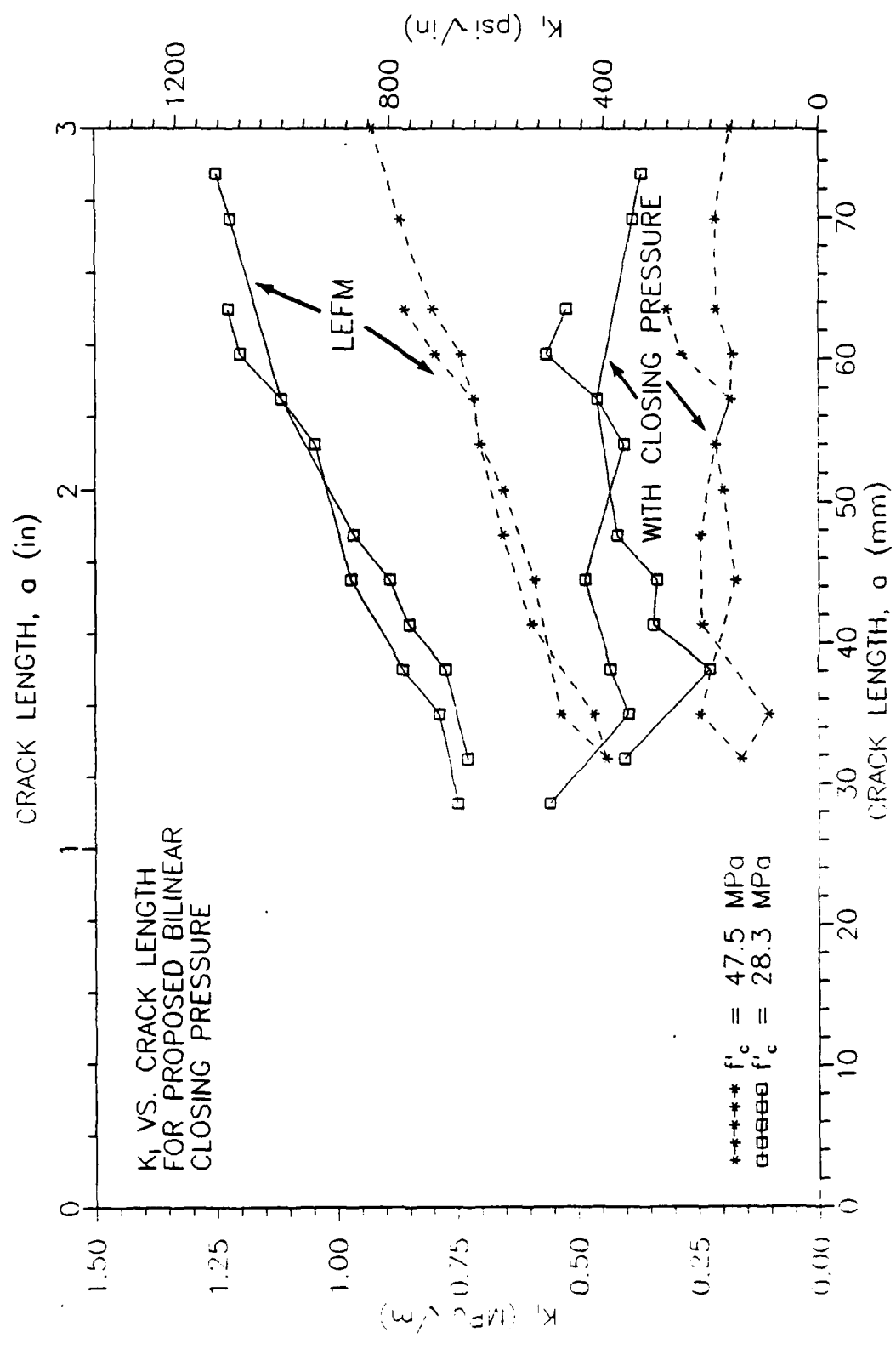
Fig. I.11. K_I vs. Crack Length for Proposed Closing Pressure.
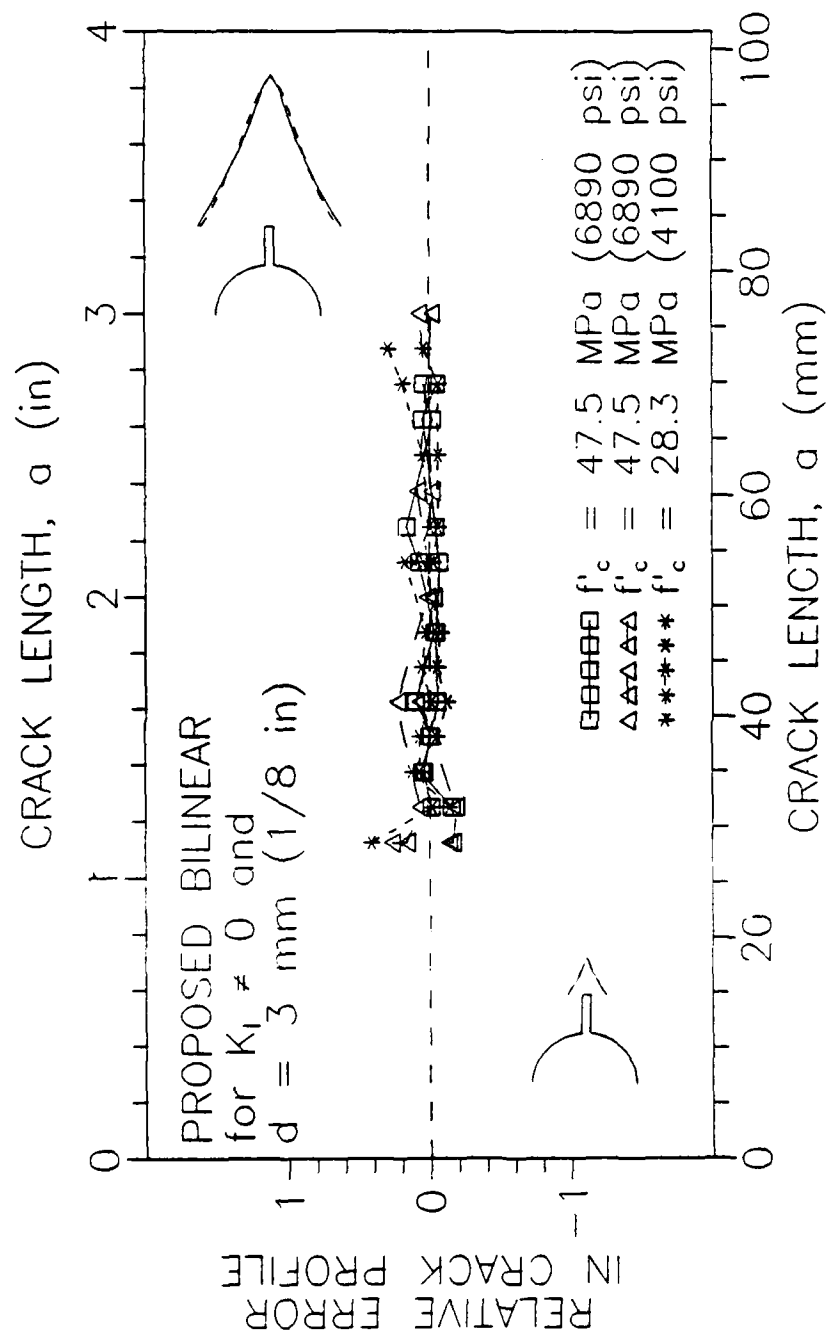
Fig. I.12. Crack Profile Comparison for Proposed Closing Pressure and $K_I \neq 0$.

1 in thickness

12 in

12 in

1 in

7/8 in

Displacement Field

Strain Field
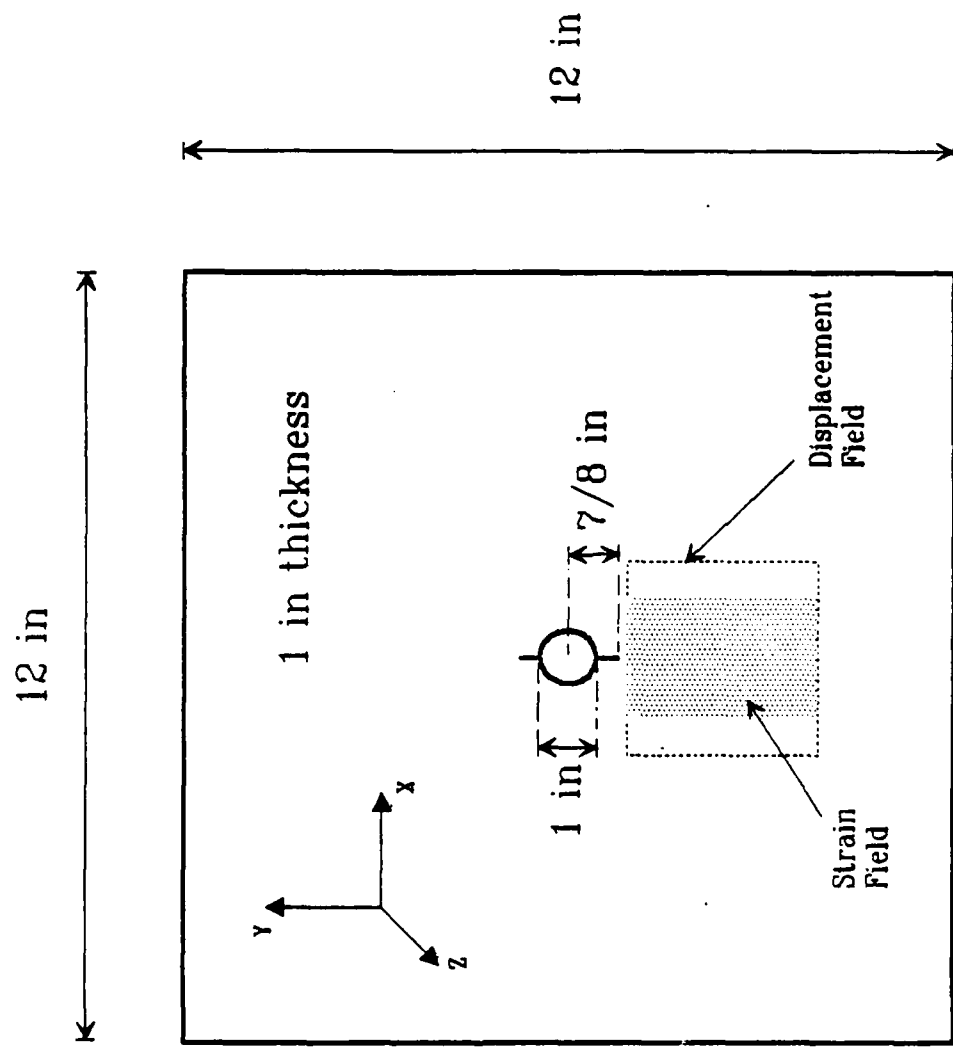
Fig. II.1. Center Notched Mortar Plate Specimen.
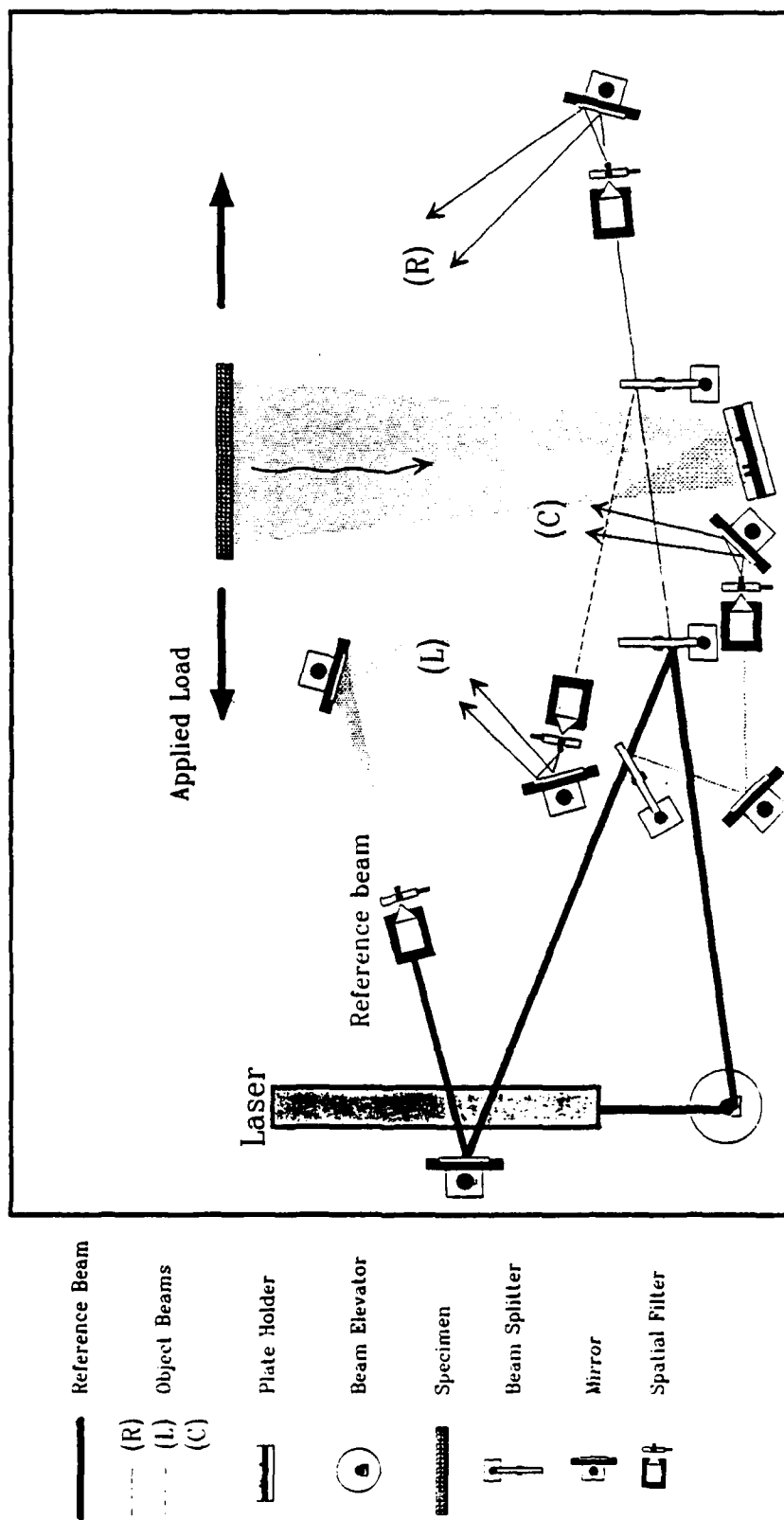
Fig. II.2. Holographic Set-up.
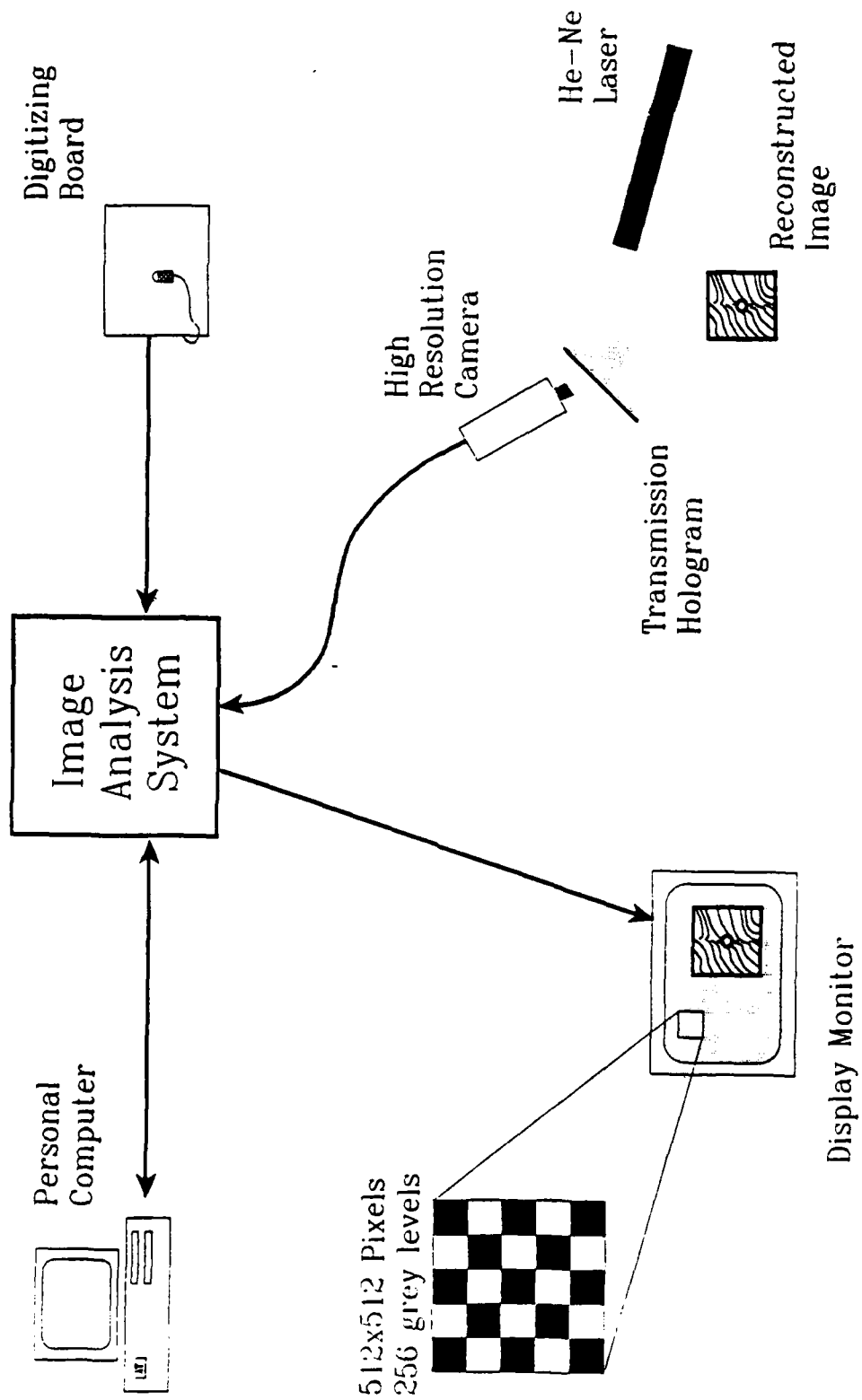
Fig. II.3.   Image Reconstruction and Acquisition Set-up.
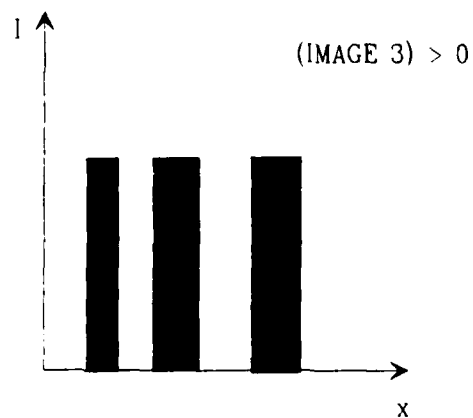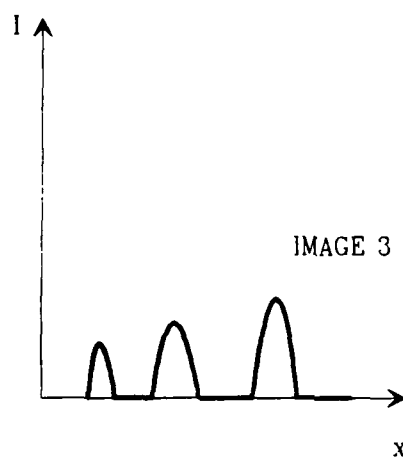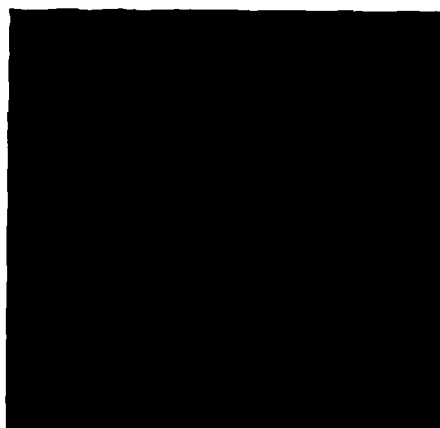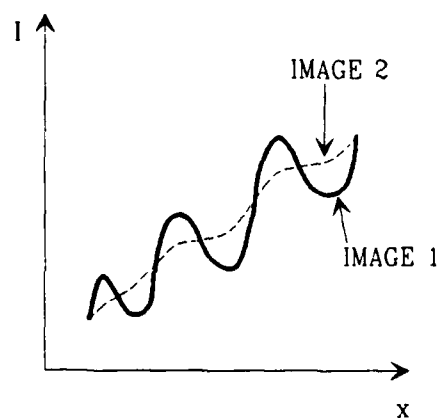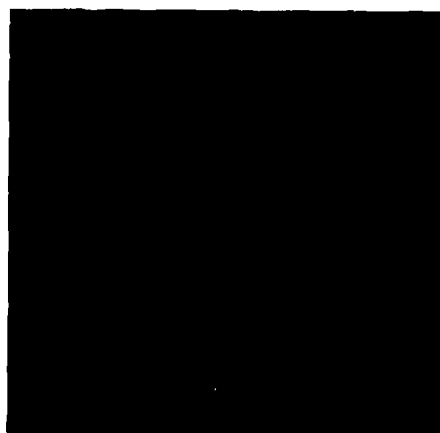
Fig. II.4a.   Intensity Distribution Across an Interferogram.
    4b.   Isolation of Interferometric Effect.
    4c.   Binary Image.

Y$_{-1}$ Y$_0$ Y$_1$

NP = 7

NP$_0$ = 10

Point A located
on this pixel

Point C (75)   Point E (65)

Point A (Intensity 65)   Point D (77)

Point F (74)

Point B (90)
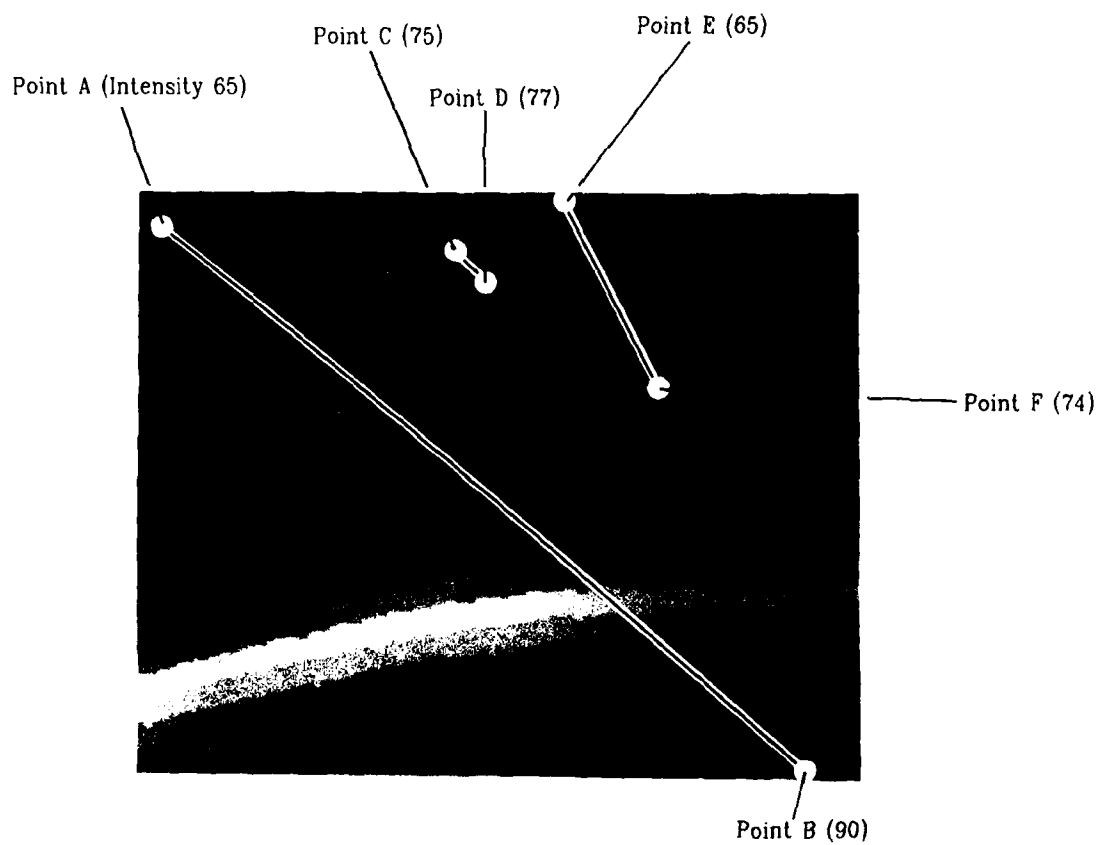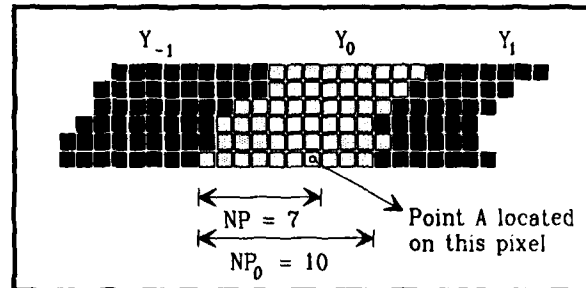
Fig. II.5.   Fringe Count by Difference in Intensity Value.

E_1 Ellipce for constant I-P-O

E_2^* Ellipce for +1/2 fringe (Δ I-P-O = $+\lambda/2$)

E_2^- Ellipce for -1/2 fringe (Δ I-P-O = $-\lambda/2$)

I   Illumination Point

O   Observation Point

P   Point on the Object

Holodiagram for two illumination directions

Several possible displacement
vectors for 1/2 fringe.

E_2^-

E_1

E_2^+

Fig. II.6.   Holodiagram.

CRACK OPENING DISPLACEMENT (microns)

CRACK LENGTH, a (mm)

CRACK PROFILE
TEST DATE 11/29/88
BOTTOM CRACK

average of holographic
measurements
(symmetry assumption)

calculated from all
three holograms

crack sliding displacement
in XZ direction

INTERPRETATION OF
HOLOGRAPHIC READINGS

P = 1601 lb

P = 1324 lb

ooooo 2-D Displacement Calculation
***** Nelson and McCrickerd (Symmetry Assumption)
------ Crack Sliding Displacement

CRACK LENGTH, a (inches)

CRACK OPENING DISPLACEMENT (10^{-5} in)

Fig. II.7. Holographically Measured Crack Profiles.

(c) Load= 1601 lb

(b) Load= 1461 lb
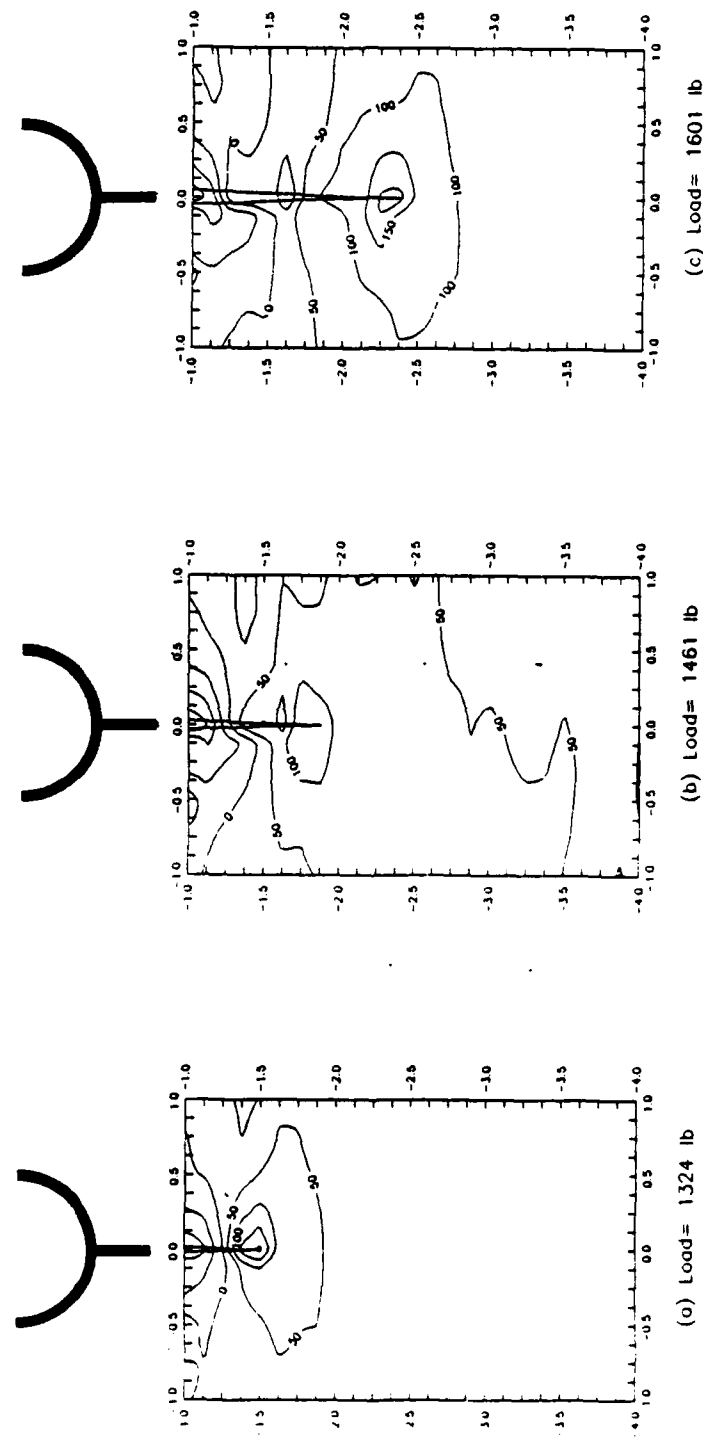
(a) Load= 1324 lb

Fig. II.8.   Holographically Measured Strain Fields.
     8a.   Crack length 1.375 in; load = 1324 lb.
     8b.   Crack length 1.875 in; load = 1461 lb.
     8c.   Crack length 2.25 in; load = 1601 lb.

$\omega_c = 20 \times 10^{-5}$ in

(a) Load = 1324 lb

$\omega_c = 34 \times 10^{-5}$ in

(b) Load = 1461 lb

$\omega_c = 62 \times 10^{-5}$ in
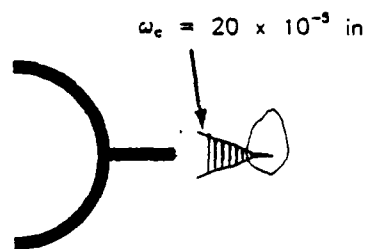
Fig. II.9.   Fracture Process Zone
   9a.   Crack length 1.375 in; load — 1324 lb.
   9b.   Crack length 1.875 in; load — 1461 lb.
   9c.   Crack length 2.25 in; load — 1601 lb.

(a) Load= 1324 lb

(b) Load= 1461 lb
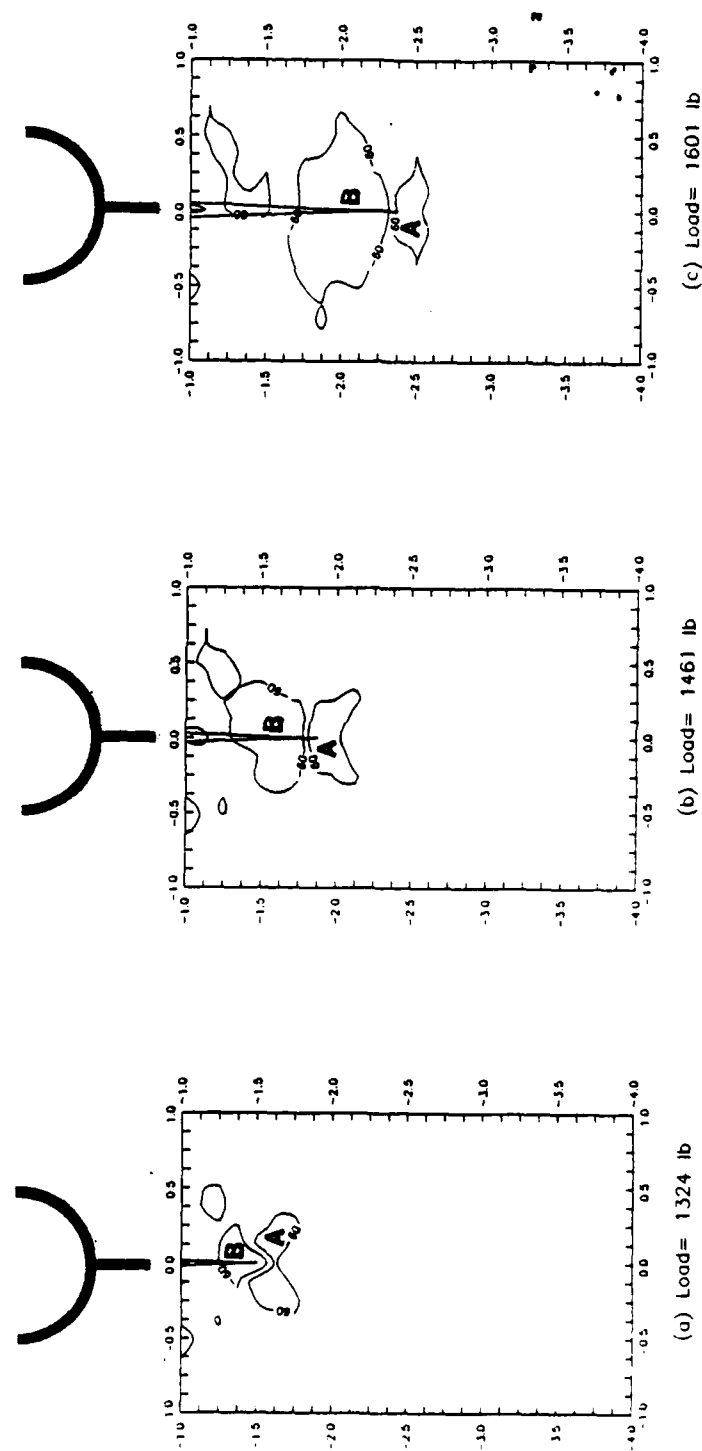
(c) Load= 1601 lb

Fig. II.10.   Difference Between Holographic and LEFM Strain Fields.
  10a.   Crack length 1.375 in; load – 1324 lb.
  10b.   Crack length 1.875 in; load – 1461 lb.
  10c.   Crack length 2.25 in; load – 1601 lb.
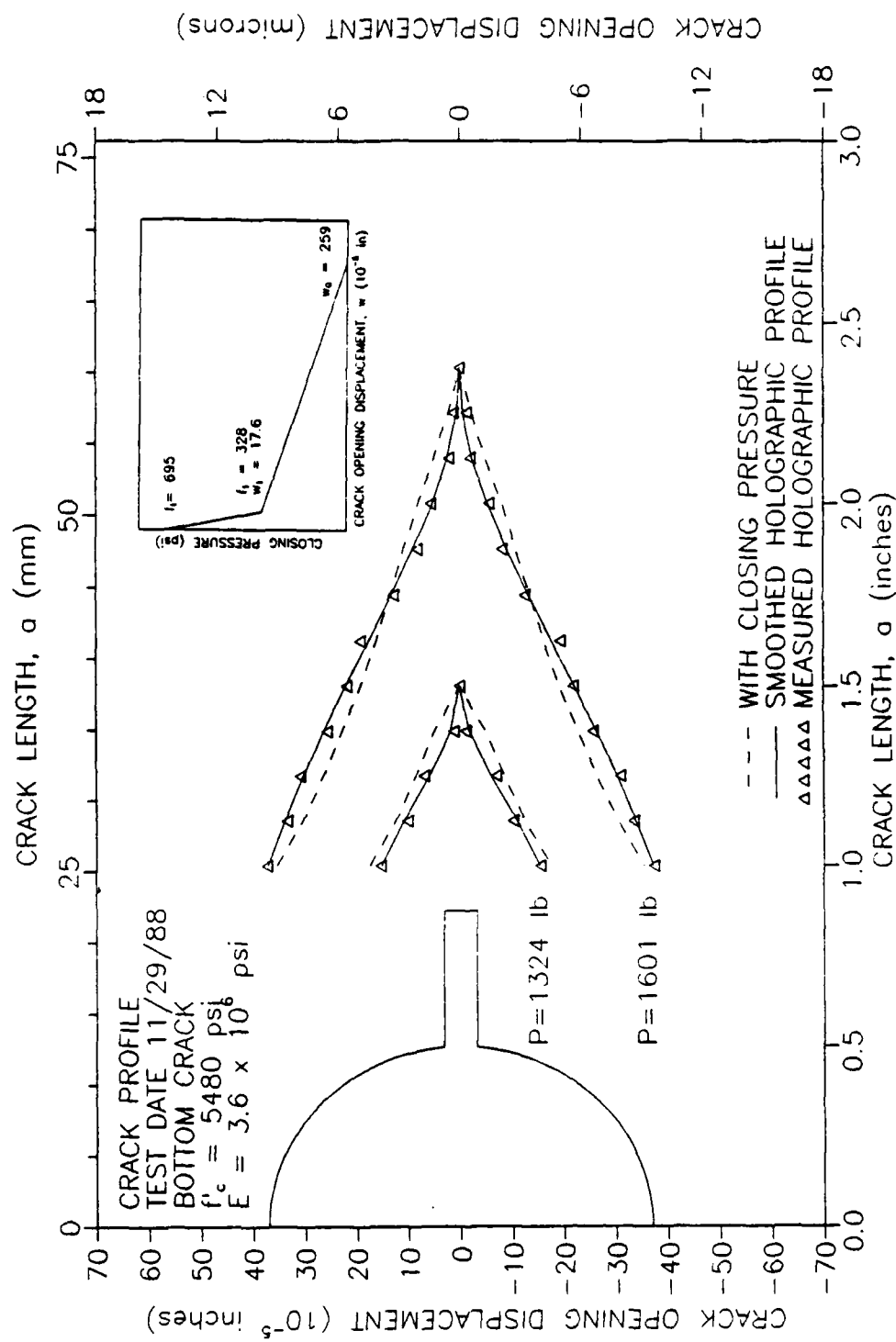
Fig. II.11. Comparison Between Holographically Obtained and Computed Crack Profiles.

(a) Load= 1324 lb

(b) Load= 1461 lb
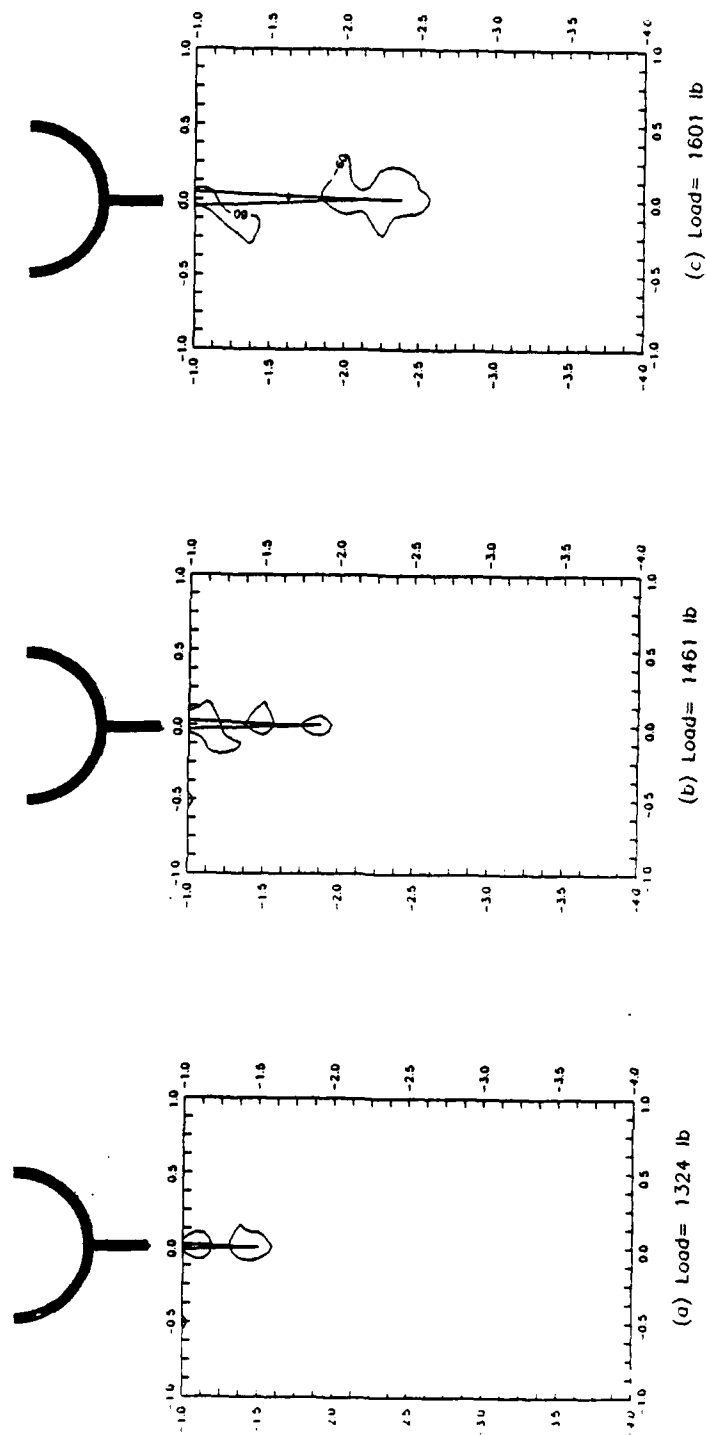
(c) Load= 1601 lb

Fig. II.12.   Difference Between Holographic and Bilinear Closing Pressure
               Strain Fields.

        12a.   Crack length 1.375 in; load = 1324 lb.
        12b.   Crack length 1.875 in; load = 1461 lb.
        12c.   Crack length 2.25 in; load = 1601 lb.
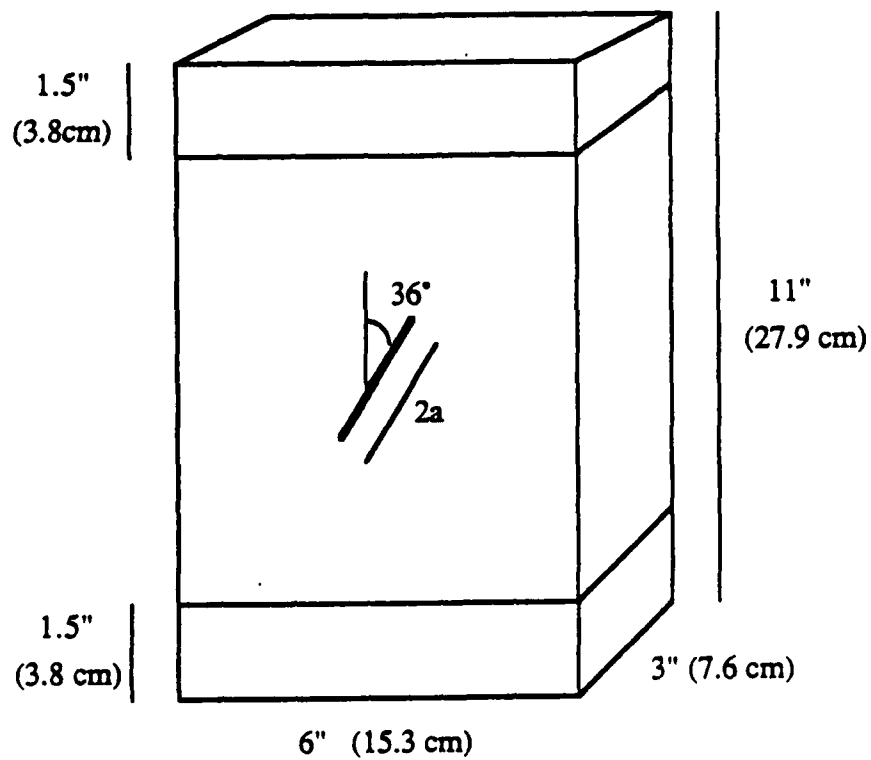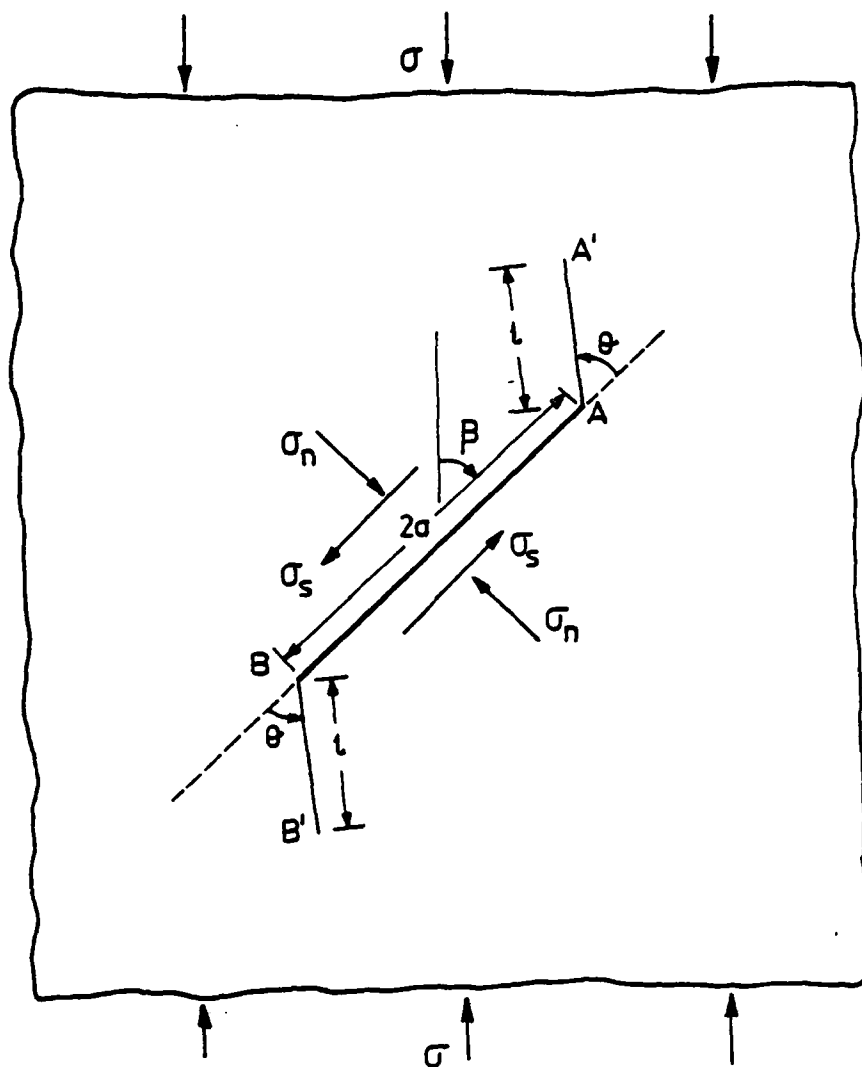
Fig. III.1.   Infinite Plate and Actual Specimen.
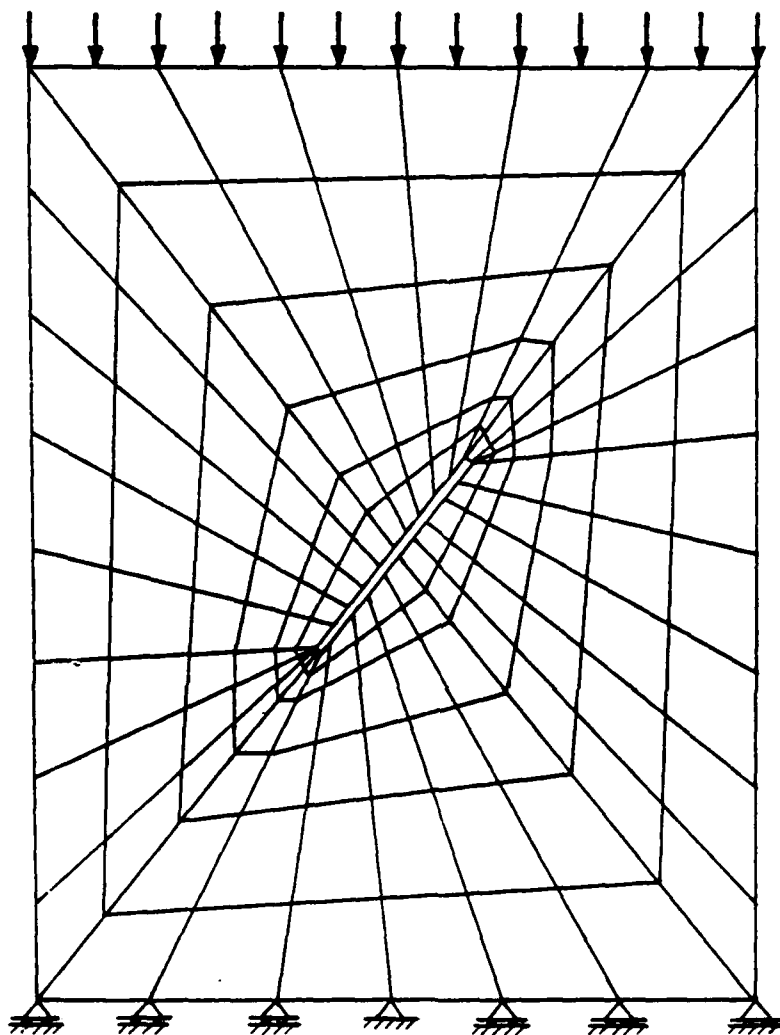
Fig. III.2.   Finite Element Mesh.
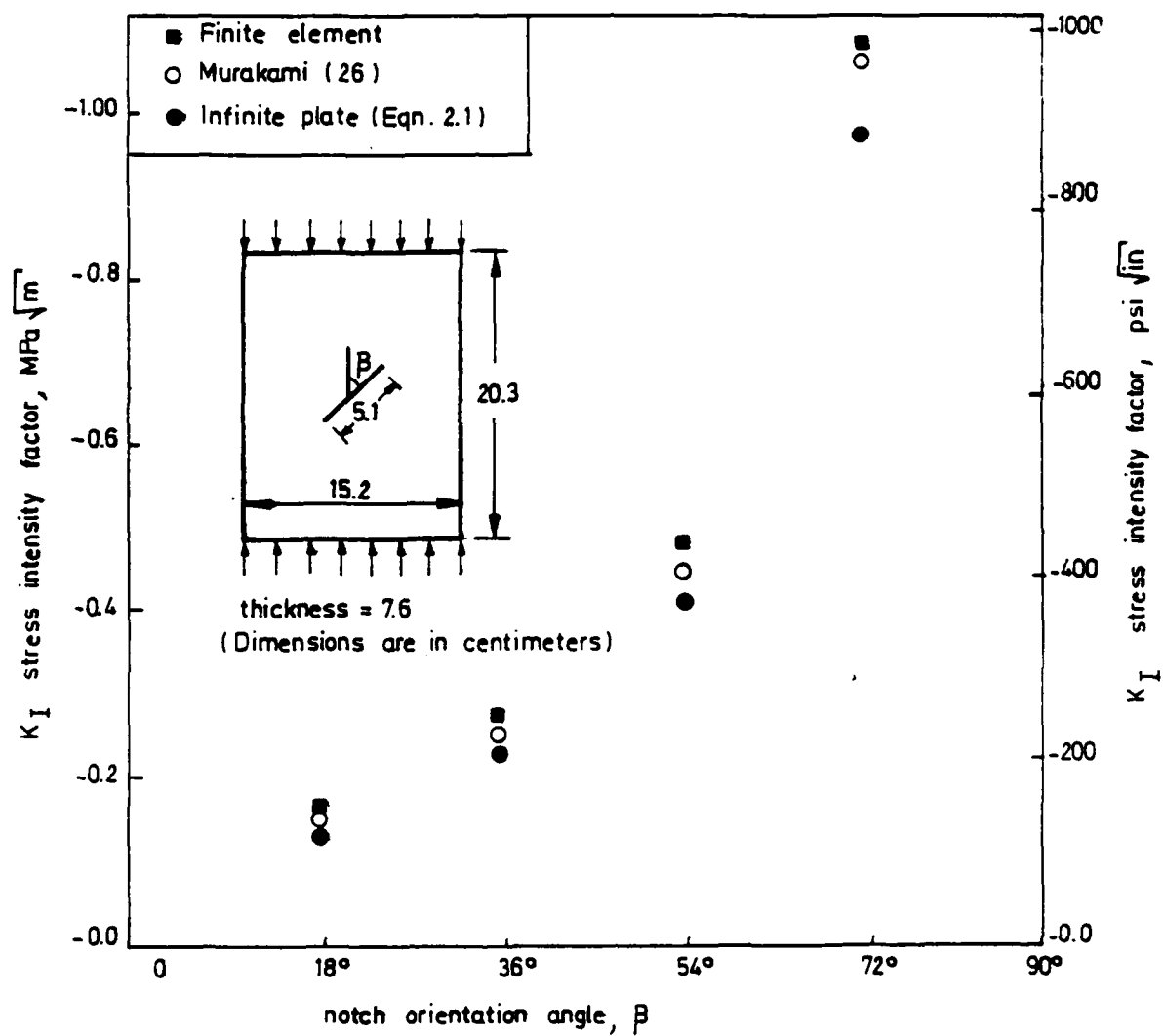
Fig. III.3.   Comparison of Different Solutions for K_I.
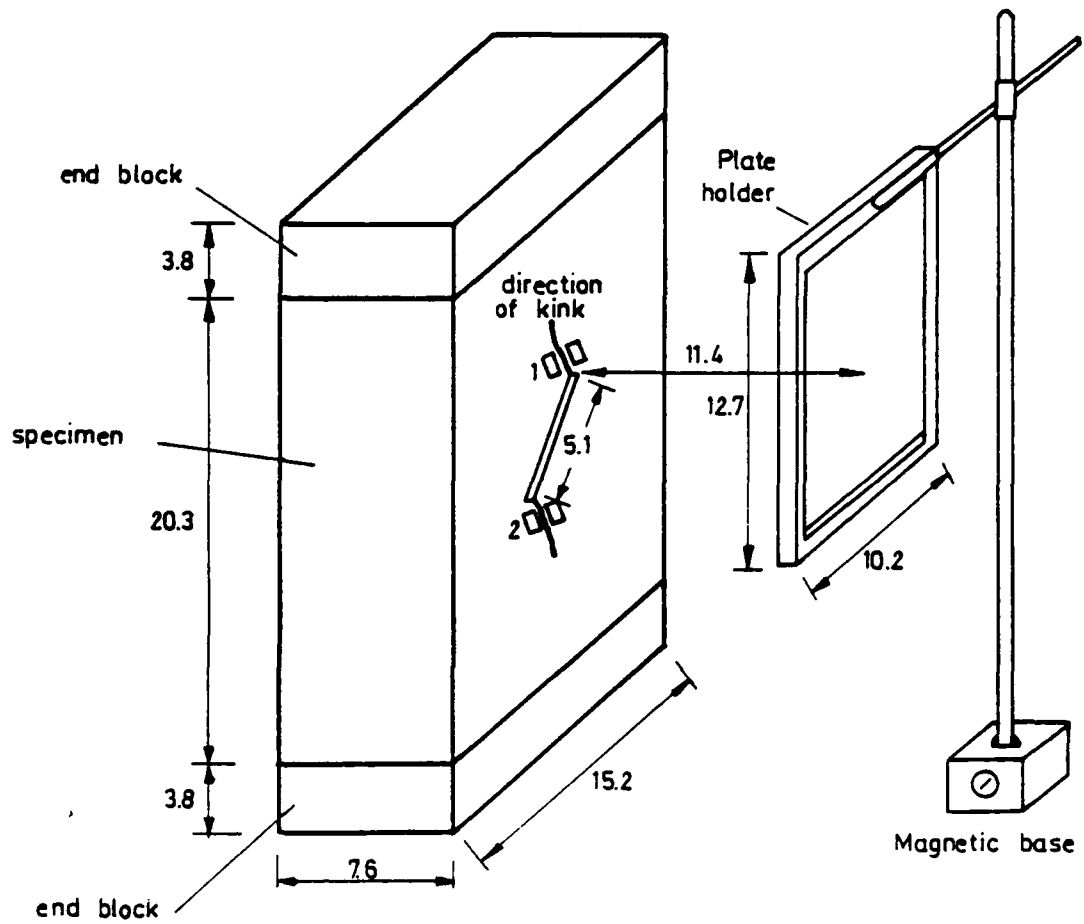
All dimensions are in centimeters,   1 cm = 0,3937 in
1 clip gages for opening
2 clip gages for sliding

Fig. III.4.   Clip Gages and Mounts.

18°   36°   54°   72°

Fig. III.5 Tested Specimens

18°

36°

54°

72°

Fig. III.6 Holographic Fringes
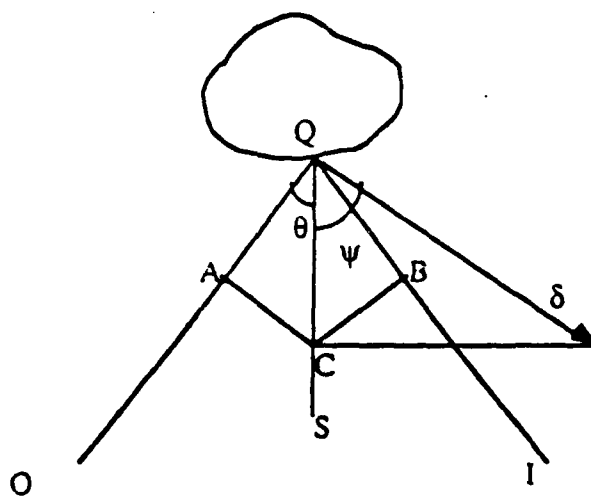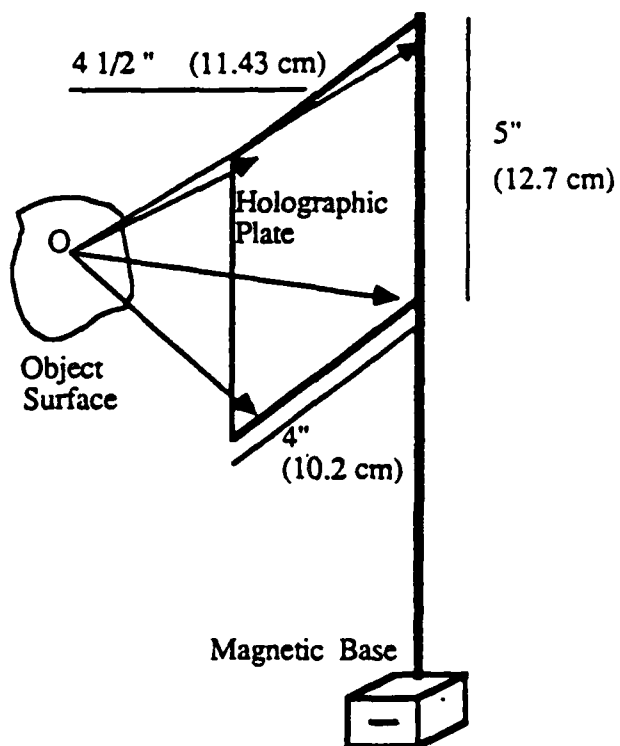
Fig. III.7.   Sensitivity of Holographic Interferometry.

Fig. III.8.   Four Observation from One Plate.
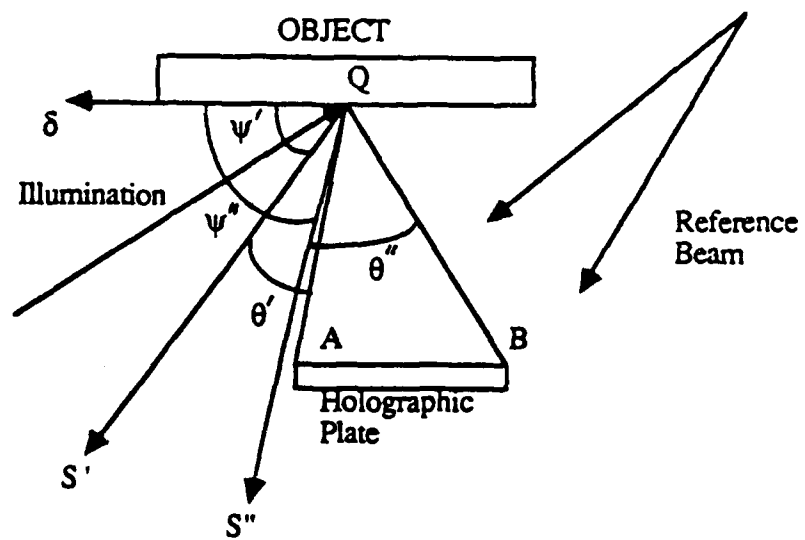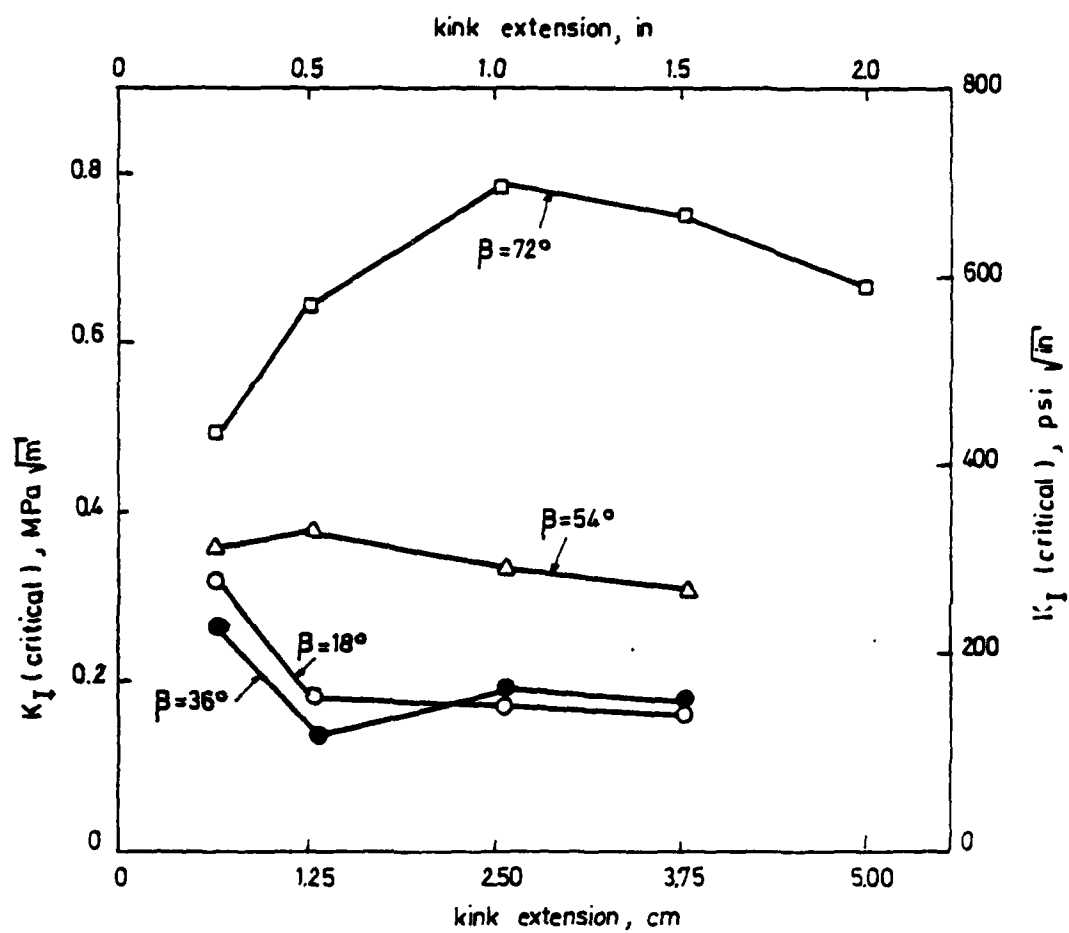
Fig. III.9.   In Plane Displacement Measurement.

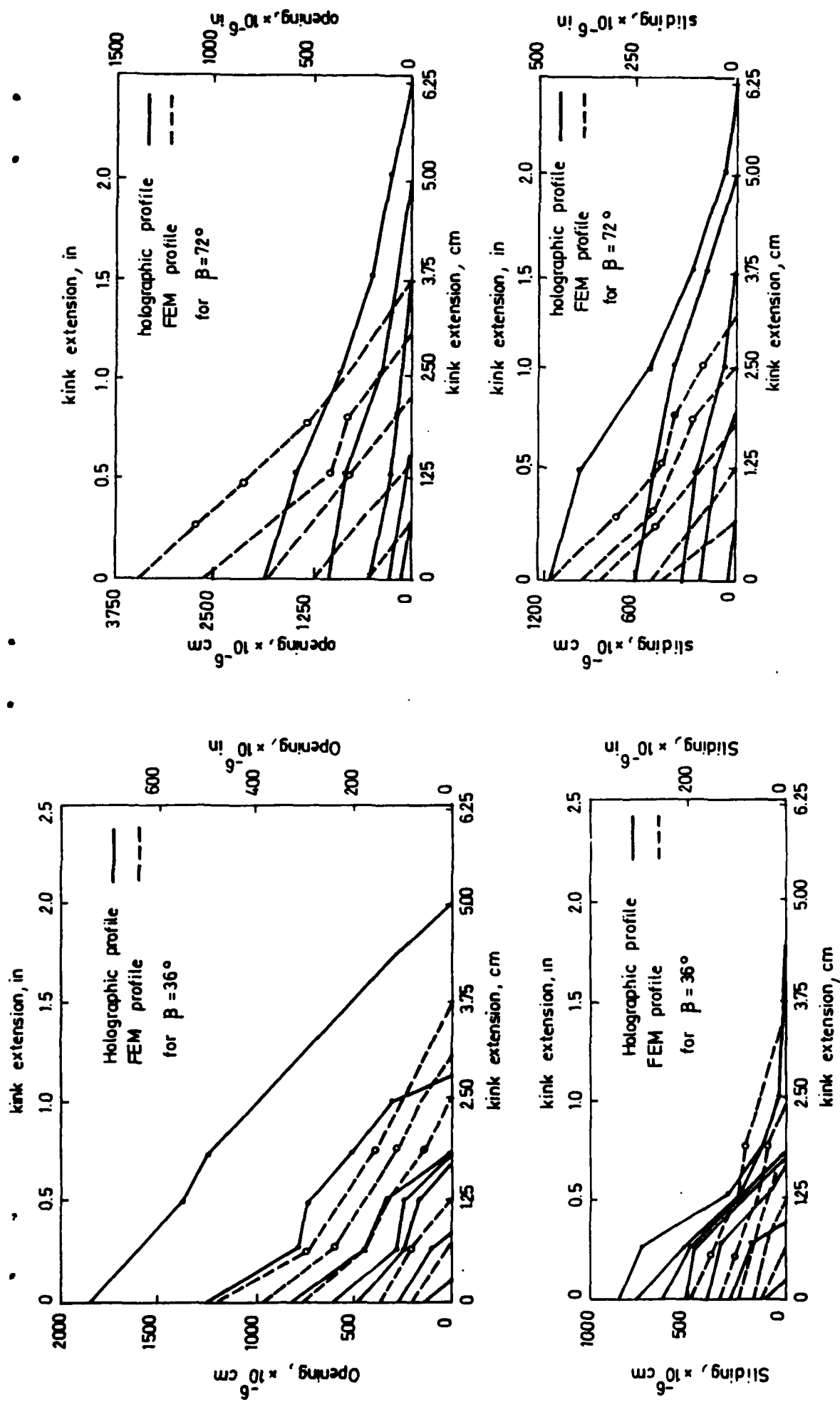Fig. III.10.   Values of K_{Ic} Before Tractions.
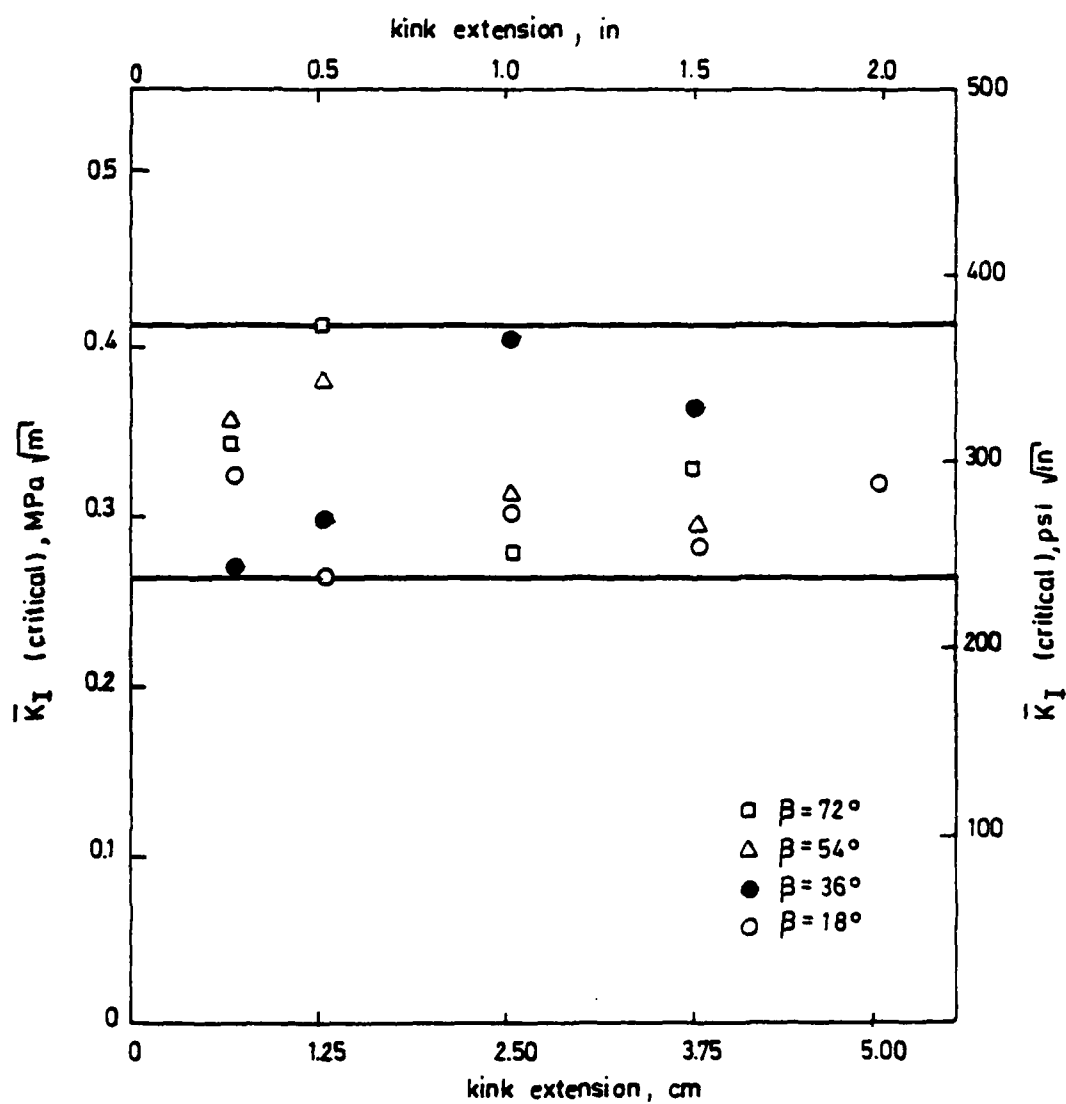
Fig. III.11.   FEM vs. Holographic Crack Profiles.

Fig. III.12.   Corrected Value of K_{Ic}.